RESEARCH ARTICLE

Key Points:
- A novel decomposition isolates how ocean surface heating, circulation changes, and air-sea interactions drive sea ice loss from CO_2 increases
- Atmosphere changes determine Arctic sea ice loss within the first decade; ocean circulation changes drive longer term ice losses
- Atmosphere-ocean coupling feedbacks on ocean circulation change in the subpolar Atlantic stabilizes Arctic sea ice loss in the long term

Supporting Information:
- Supporting Information S1

Correspondence to:
O. A. Garuba,
Oluwayemi.Garuba@pnnl.gov

Disentangling the Coupled Atmosphere-Ocean-Ice Interactions Driving Arctic Sea Ice Response to CO_2 Increases

Oluwayemi A. Garuba[1] , Hansi A. Singh[2] , Elizabeth Hunke[3] , and Philip J. Rasch[1]

[1]Pacific Northwest National Laboratory, Richland, WA, USA, [2]School of Earth and Ocean Sciences, University of Victoria, Victoria, British Columbia, Canada, [3]Los Alamos National Laboratory, US Department of Energy Office of Science, Los Alamos, NM, USA

Abstract A novel decomposition of the ocean heat energy that contributes to sea ice melt and growth (ocean-ice and frazil heat) into components that are driven by surface heat flux and ocean circulation changes is used to isolate the evolving roles of the atmosphere and ocean in the Arctic sea ice loss from CO_2 increases. A sea ice volume budget analysis is used to separate the impacts of the anomalous frazil/ocean-ice heat from those of atmosphere-ice heat on the evolving Arctic sea ice volume. The role of atmosphere-ocean coupling in augmenting or curtailing the atmosphere- and ocean-driven sea ice losses is further isolated by comparing the ice volume budget and the anomalous frazil/ocean-ice heat components in partially and fully coupled experiments. Atmosphere-ice heat fluxes drive most of Arctic sea ice loss in the first decade following CO_2 increase by increasing the sea ice top face melt in summer, while ocean circulation changes drive the loss over the longer term through the anomalous increase of heat transport into the Arctic, which drive decreases in frazil ice growth and sea ice extent in winter. Atmosphere-ocean coupling in the subpolar Atlantic further supports a negative feedback that attenuates the ocean-driven sea ice losses over time; by accelerating the weakening of the Atlantic meridional overturning circulation, it causes a large cooling of the subpolar Atlantic and attenuation of the anomalous heat transport into the Arctic in winter, allowing for a seasonal Arctic sea ice in the fully coupled experiment, while the Arctic completely becomes ice free in the partially coupled experiment.

Plain Language Summary The interactions between the atmosphere, ocean, and sea ice are disentangled in order to isolate their individual roles in driving Arctic sea ice losses and how these roles change over time. We introduce a new decomposition of the ocean heat that contributes to melting and growing sea ice into parts that are caused by changes in the surface heat input into the ocean and ocean circulation. We analyze the contributions of the ocean heat and atmosphere heat to the overall Arctic sea ice volume changes, both in an experiment where a two-way interaction between the atmosphere and ocean is allowed and in another where this two-way interaction is not allowed. Our results suggest that the atmosphere causes most of Arctic sea ice loss (within a decade) by increasing sea ice top face melt, while the ocean causes the long-term sea ice changes in the Arctic by decreasing winter bottom face growth. The interactions between the atmosphere and ocean further enhance the ocean circulation weakening and surface cooling in the subpolar Atlantic and thereby stop the winter heat transport increase into the Arctic and eventually curtail the ocean-driven sea ice loss and prevent the total loss of Arctic sea ice.

1. Introduction

Sea ice loss due to anthropogenic greenhouse gas emissions is a coupled process involving a complex series of interactions between the atmosphere, ocean, and sea ice on a range of temporal and spatial scales. Ultimately, sea ice loss with greenhouse gas forcing is driven by anomalous atmosphere and ocean heat fluxes that, in concert, decrease sea ice growth and increase sea ice melt (Bitz et al., 2005; Gabison, 1987; Semtner, 1976).

Anomalous atmospheric heat fluxes at the top surface of the ice are determined by atmospheric radiative and turbulent flux changes, which are, in turn, influenced by changing atmospheric energy transport, radiative feedbacks, clouds, and chemical composition (Goosse et al., 2018; Hwang et al., 2011; Kay et al., 2008, 2012; Singh et al., 2018). Anomalous ocean heat fluxes, acting on the bottom or lateral edges of the ice, may arise

from changing heat input into the ocean or from changing ocean circulation and mixing processes (Bitz et al., 2005; Martinson & Iannuzzi, 1998; Mayer et al., 2016; Winton, 2003). These atmospheric and oceanic changes are also influenced by air-sea coupling, which can further augment or curtail them. Changes in sea ice also alter surface heat and freshwater fluxes that can further impact the ocean circulation and mixing processes (Bitz et al., 2006; Liu et al., 2019; Svellec et al., 2017). Other interactions, particularly ice-albedo feedback and the ice-thickness feedback, can further accelerate or decelerate this coupled response (Bitz & Roe, 2004; Curry et al., 1995).

These coupled interactions between atmosphere, ocean, and sea ice make attribution and prediction of sea ice changes challenging. The proximity of the Arctic to the amplified atmospheric warming in the Northern Hemisphere and the meridional overturning circulation and its large ocean heat transport in the Atlantic make it a hot spot for coupled interactions. It is unclear what the relative roles of atmospheric and oceanic fluxes are in driving sea ice loss and how these roles may evolve with time (Holland et al., 2006; Serreze et al., 2007; Stroeve et al., 2012). Coupled climate models often disagree on the extent to which the ocean and atmosphere instigate sea ice retreat (Bracegirdle et al., 2018; Burgard & Notz, 2017; Holland et al., 2010). Several studies have suggested that changes in atmospheric radiative fluxes (particularly surface longwave input) and circulation play an important role in sea ice loss (Francis & Hunter, 2006; Kay et al., 2008; Maslanik et al., 2007; Stroeve et al., 2007, 2012). However, other studies have also demonstrated that meridional ocean heat transport changes play a role in Arctic sea ice loss, both in instigating abrupt changes and augmenting predictability over longer time scales (Årthun et al., 2019; Auclair & Tremblay, 2018; Dmitrenko et al., 2008; Holland et al., 2006; Nummelin et al., 2017; Polyakov et al., 2005, 2017; Walczowski & Piechura, 2006; Yeager et al., 2015). Therefore, disentangling various components of the coupled atmosphere-ocean-ice interactions is important for improved understanding and predictability of sea ice loss and for diagnosing coupled climate model projections of sea ice changes.

Earlier studies have isolated the contributions of anomalous surface heat fluxes and ocean heat transport and storage and anomalous melt and growth to the overall sea ice volume change. Bitz et al. (2005) and Winton (2003) highlighted the importance of the ocean circulation strength and heat convergence in setting the sea ice extent. Ding et al. (2016) also used an ocean heat content budget to isolate the roles of ocean heat storage and anomalous surface heat fluxes in determining the seasonal cycle sea ice in the Arctic. Their results suggest that anomalous surface heat fluxes play a primary role in the seasonal changes, while ocean heat convergence only plays a secondary role in the Arctic. A sea ice volume budget analysis is also used in the multimodel and single-model analysis of Holland et al. (2010), West et al. (2013), and Keen and Blockley (2018) to understand the relative roles of melt and growth changes in sea ice loss. They found that increase in the melt is important in the short term, while growth decrease becomes important in the long term. However, the roles of the atmosphere and ocean in driving these anomalous surface heat fluxes or ocean heat storage or melt and growth changes that cause Arctic sea ice loss are not clearly defined in these previous studies.

In this study, we present a novel decomposition of the anomalous ocean heat energy that contributes to sea ice melt and growth changes (ocean-ice and frazil heat) in fully and partially coupled CO_2-quadrupling experiments. A passive tracer decomposition method introduced in the studies of Banks and Gregory (2006) and Xie and Vallis (2012), is used to decompose the anomalous ocean temperature into components that are driven by surface heat flux anomalies and ocean circulation changes, respectively. The anomalous ocean temperature components are then also used to isolate the frazil/ocean-ice heat components that are driven by surface heat flux and ocean circulation changes. In order to identify sea ice volume changes that are driven by atmosphere-ice heat fluxes (atmosphere-driven) and frazil/ocean-ice heat (ocean-driven), the contributions of the anomalous melt and growth rates at the sea ice top and bottom faces to the evolving sea ice volume budget are first analyzed. The frazil/ocean-ice heat decomposition is then used to isolate the roles of anomalous surface heat fluxes and ocean-circulation changes in ocean-driven sea ice changes. A partially coupled experiment wherein the impact of ocean circulation changes on the air-sea interaction is suppressed is further used to access the role of the coupling between the atmosphere and ocean in augmenting or curtailing the atmosphere- and ocean-driven sea ice volume changes. The formulation and validation of the partial coupling method are described in detail in the study of Garuba and Rasch (2020) (hereafter GR20). By comparing the evolving Arctic sea ice volume

budget and frazil/ocean-ice heat components in the fully and partially coupled experiments, we discern the time-evolving roles of the atmosphere, ocean, and the coupling between them in driving sea ice loss in the Arctic.

2. Experimental Design and Method Formulation

2.1. Model and Experiments

This study uses the Community Earth System Model version 1.2 (CESM 1.2) global coupled model. CESM 1.2 consists of the Community Atmospheric Model version 5 (CAM5) (Neale et al., 2010), the Parallel Ocean Program version 2 (POP2) (Danabasoglu et al., 2012), the Community Land Model version 4 (CLM4) (Oleson et al., 2010), and the Community Ice CodE (CICE) (Hunke et al., 2010). The horizontal resolution used for CAM5 and CLM4 is $1.5° \times 0.9°$, with the atmospheric component having 30 vertical levels. CICE and POP are run on a nominally 1°-resolution, displaced-pole grid (with the north pole singularity centered over Greenland); POP has 61 vertical levels.

The methodology uses three simulations, a control simulation used to define the baseline model behavior, and two perturbed simulations in which CO_2 is quadrupled. In the first perturbed run (called the "fully coupled experiment"), the standard atmosphere-ocean coupling is used. In the second perturbed experiment (called the "partially coupled experiment"), the impact of ocean circulation anomalies in the atmosphere-ocean coupling is suppressed (described in detail in section 2.2.4). Both perturbed simulations are initialized from a 1000-year equilibrated control simulation with preindustrial CO_2 concentrations and integrated forward in time for 100 years following the abrupt quadrupling of atmospheric CO_2 concentrations from 284 to 1,136 ppm. CO_2-induced anomalies are defined as the difference between the perturbed and preindustrial control experiment states. A set of temperature-like tracers is added to the fully and partially coupled perturbed experiments to decompose the anomalous ocean temperature, frazil heat, and ocean-ice heat fluxes into components that are driven by surface heat flux anomalies and ocean circulation changes, respectively (described in detail in sections 2.2.2 and 2.2.3). The sea ice volume budget and anomalous frazil/ocean-ice heat flux components in the partially and fully coupled experiments are compared to isolate the role of atmosphere-ocean coupling in modifying the atmosphere- and ocean-driven sea ice changes.

2.2. Disentangling the Coupled Atmosphere-Ocean-Ice Interaction

2.2.1. Governing Equations

The rates of sea ice growth and melt at the atmosphere-ice (top) and ocean-ice (bottom) interfaces are described by the thermodynamic equations (Bitz et al., 2005; Hunke et al., 2010):

$$-q\frac{\partial h}{\partial t}\Big|_{top} = F_{AI} - I_o - k\frac{\partial T_I}{\partial z}, \tag{1}$$

and

$$-q\frac{\partial h}{\partial t}\Big|_{basal} = -F_{OI_b} + k\frac{\partial T_I}{\partial z}, \tag{2}$$

$$-q\frac{\partial h}{\partial t}\Big|_{new} = -F_i. \tag{3}$$

Here h is the ice area weighted sea ice thickness; $\frac{\partial h}{\partial t}$ is the rate of ice growth or melt; q is the enthalpy of sea ice; I_O is the solar radiation that passes through the upper surface of the ice; k is the conductivity of the ice; $\frac{\partial T_I}{\partial z}$ is the vertical temperature gradient at the sea ice top and bottom layers, respectively; F_{AI} are the atmosphere-ice heat fluxes (radiative and turbulent; can be positive or negative) that can cause melt at the ice top face or basal growth at the ice bottom face by heat conduction through ice; F_{OI_b} is the ocean heat that is used for basal melt at the ice bottom face; additional ocean heat is also used to melt sea ice laterally (F_{OI_l}), so that the net ocean-ice heat fluxes used for melt is $F_{OI} = F_{OI_b} + F_{OI_l}$; F_{OI} is always negative, and F_{AI} and F_{OI} are weighted by sea ice area; F_i is the frazil heat, that is, the latent heat release when new ice forms over

open waters (frazil ice growth), where ocean temperatures momentarily fall below the freezing temperature or supercools. F_i is also equivalent to the heat energy required to keep the ocean temperature from falling below freezing where frazil ice forms; F_i is thus always positive (sign convention is positive downward). Equations 1–3 are solved by the sea ice model to compute the sea ice thickness changes that occur at the sea ice top and bottom faces, respectively. Further adjustments to sea ice thickness within the ice layers due to brine pockets and ice dynamics are computed in the sea ice model that are not included in Equations 1–3, but these adjustments do not change the overall energy budget of sea ice that is considered in this study.

Frazil and ocean-ice heat (F_i/F_{OI}) are both derived from a quantity called the freezing/melting potential (F_{IOI}), which is computed as a function the departure of the ocean temperature from the freezing temperature:

$$F_{IOI} = c_w(T_{frz} - T_O|_s).$$

(4)

Here $T_O|_s$ is a *provisional* estimate of the ocean surface temperature field, T_{frz} is the freezing temperature of seawater (a constant $-1.8°C$ in the CESM 1.2), and c_w is the heat capacity of the ocean top layer. As indicated by Equation 4, F_{IOI} is positive where the provisional ocean surface temperature drops below freezing (i.e., $F_{IOI} > 0$ where $T_{frz} > T_O|_s$) and negative where it is above freezing ($F_{IOI} < 0$ where $T_{frz} < T_O|_s$). Positive values of F_{IOI} thus represent the freezing potential that is used for frazil ice growth (i.e., $F_i = F_{IOI} > O$), while negative values of F_{IOI} represent the melting potential that may be used for basal or lateral sea ice melt. Note that $F_{IOI} < 0$ almost everywhere but can only be used for melt where ice is available; where ice is available, some or all of F_{IOI} may be used for melt depending on the magnitude of the conductive term in Equation 2; F_{OI} is the actual amount of the negative values of F_{IOI} that is used for melt where ice is available (i.e., $F_{OI} \geq F_{IOI} < 0$; Hunke et al., 2010).

For the purposes of calculating the freezing/melting potential and decomposing the frazil heat and ocean-ice heat fluxes, a *provisional* ocean temperature estimate is used. The provisional ocean temperature estimate is the ocean temperature value "before" it is adjusted for ice growth or melt. The ocean temperature has to be further adjusted to account for sea ice growth and melt after the values of F_i and F_{OI} are determined as the ocean temperature does not depart from the freezing temperature when sea ice growth and melt occurs physically. The provisional ocean temperature change may be described with the tendency equation:

$$\frac{\partial T_O}{\partial t} = Q - v \cdot \nabla T_O.$$

(5)

Here, T_O is the three-dimensional ocean temperature field and Q is the two-dimensional atmosphere-ocean surface heat flux field exchanged over open waters (positive downward into the ocean and nonzero only at the surface layer); v is the three-dimensional ocean circulation field, representing all ocean transport processes including resolved advection, horizontal diffusion, and vertical mixing. Equation 5 is also normalized by the heat capacity (c_w) for simplicity, so that Q has units of Deg s^{-1}.

Since it has not accounted for sea ice growth or melt, the provisional or numerical ocean temperature can go below freezing or above freezing (where ice is available) due to surface heat loss or ocean heat convergence below the ice and thereby allows F_{IOI} to include both positive and negative (where ice is available) values according to Equation 4. These positive and negative values may then be used to account for frazil ice growth or sea ice melt as F_i and F_{OI}, respectively. The provisional ocean temperature is then reset to the freezing temperature where frazil ice growth occurs or sea ice remains after the melting potential has been applied to melt ice. F_{OI} and F_i are the equivalent amount of heat energy needed to adjust the ocean temperature for ice melt and frazil ice growth, respectively.

The actual adjusted ocean temperature change is thus described by the tendency equation:

$$\frac{\partial T_O}{\partial t} = Q + F_{OI} + F_i - v \cdot \nabla T_O.$$

(6)

The provisional ocean temperature estimate is critical to the frazil/ocean-ice heat decomposition described in this study as it contains the information of the ocean temperature change that contribute to sea ice melt or growth. This information is lost after the ocean temperature is adjusted for ice growth or melt, since T_O would be equal to T_{frz} and F_{IOI} would be zero where ice present or frazil ice forms. The provisional ocean temperature components are thus what can be used for decomposing F_{OI} and F_i into components, respectively. The decomposition of the provisional ocean temperature (Equation 5) with tracers is described in section 2.2.2; the frazil/ocean-ice heat flux is then decomposed using the resulting provisional tracer components (section 2.2.3). The provisional tracer components are similarly adjusted for growth and melt with their respective contributions to F_{OI} and F_i after F_{OI} and F_i are decomposed.

For those interested in and familiar with specific details of the CESM coupled model, it is important to note that because F_{OI} is added to Q to compute the ocean temperature change at the start of the coupling interval, it may appear that the provisional ocean temperature tendency that is used for computing the freezing/melting potential (Equation 5) should already include F_{OI}. However, the addition of F_{OI} at the start of the coupling interval is not inconsistent with Equation 5; it serves to complete iteration of the ocean temperature tendency from the previous coupling time interval, adjusting it for melt. This is done because the information on ice accumulation is only available in the sea ice model, such that the ocean temperature can only be adjusted for frazil ice growth and ice melt at the different coupling time intervals (Smith et al., 2010). The ocean temperature (T_{O_t}) change due to the air-sea surface heat fluxes (Q_t) is adjusted for freezing with the frazil heat (F_{i_t}) within the same coupling interval, right after the freezing/melt potential (F_{IOI_t}) is computed, while it is adjusted for melt in the next coupling time interval after the actual amount of F_{IOI_t} used for melt (F_{OI_t}) is received from the sea ice model. F_{OI_t} is then added to the surface heat fluxes in the new coupling time interval (Q_{t+1}) to compute the provisional ocean temperature at the new time ($T_{O_{t+1}}$). The addition of F_{OI_t} to Q_{t+1} thus serves to adjust T_{O_t} rather than $T_{O_{t+1}}$, and $T_{O_{t+1}}$ at the time is used to compute $F_{IOI_{t+1}}$, can still be described with the discretized form of tendency Equation 5, and can still go above freezing where ice is present. In standalone mode, ice accumulation is saved in the ocean model, and the ocean temperature is adjusted for growth and melt within the same coupling time interval.

2.2.2. Ocean Temperature Decomposition

As indicated by Equations 1 and 4, the ocean plays a crucial role in the sea ice volume evolution; sea ice growth is initiated with frazil ice formation resulting from the supercooling of ocean temperatures, and sea ice melt resulting from ocean-ice heat fluxes also determines the overall rate of sea ice thickness changes. Therefore, understanding the ocean processes that drive frazil/ocean-ice heat flux changes is necessary to understand the net sea ice volume evolution. According to Equations 4 and 5, frazil/ocean-ice heat fluxes changes, as computed in this model, are driven only by the provisional ocean temperature changes (T_{frz} is constant); ocean temperature changes, in turn, depend on surface heat flux and ocean circulation or heat transport changes. Therefore, the contributions of anomalous surface heat fluxes and ocean circulation changes to the frazil/ocean-ice heat flux changes can be isolated by decomposing the provisional ocean temperature anomalies in a perturbed experiment. To see this, consider the equation describing the evolution of the provisional ocean temperature anomaly in a perturbed experiment, derived by taking the difference between the perturbed (Equation 5) and baseline provisional ocean temperature tendency equations. The provisional baseline ocean temperature tendency is given as

$$\frac{\partial \overline{T}_O}{\partial t} = \overline{Q} - \overline{v} \cdot \nabla \overline{T}_O. \tag{7}$$

The difference between (5) and (7) is equivalent to the tendency equation for the provisional ocean temperature change in a perturbed experiment:

$$\frac{\partial T'_O}{\partial t} = Q' - v' \cdot \nabla \overline{T}_O - v \cdot \nabla T'_O. \tag{8}$$

Here, overbars denote baseline variables (from a control experiment); variables without prime or overbars denote perturbed variables (from a perturbed experiment), and primes denote the difference between perturbed and baseline variables (i.e., $T_O = \overline{T}_O + T'_O$; $Q = \overline{Q} + Q'$; $v = \overline{v} + v'$). Equation 8 shows that the

sources of ocean temperature changes are the anomalous surface heat fluxes Q' and ocean circulation changes v', denoted by the first two terms; the third term represents the ocean transport of the temperature anomalies rather than a source term. Equation 8 can be decomposed based on these source terms into two parts that sum up to the original equation, that is,

$$\frac{\partial T'_{OQ}}{\partial t} = Q' - v \cdot \nabla T'_{OQ},\tag{9}$$

and

$$\frac{\partial T'_{OO}}{\partial t} = -v' \cdot \nabla \overline{T}_O - v \cdot \nabla T'_{OO}.\tag{10}$$

Here, $T'_O = T'_{OQ} + T'_{OO}$, so that Equations 9 and 10 sum up to Equation 8. T'_{OQ} denotes the "surface-driven" anomalous ocean temperature component that is caused by anomalous surface heat fluxes, while T'_{OO} denotes the "circulation-driven" component, caused by ocean circulation changes. By definition, T'_{OO} does not cause a net change in the global ocean heat content because it is due to the rearrangement of the baseline temperature ($\overline{T}_O$) gradients by ocean circulation changes (v'), but T'_{OO} can contribute large heat content changes regionally. Each anomalous temperature component is also subject to ocean transport processes ($v \cdot \nabla T'_{OQ}$ and $v \cdot \nabla T'_{OO}$) so that anomalous temperature components at a given location can include the impact of both local and remote surface heat flux and ocean circulation changes.

These anomalous ocean temperature components are isolated using a tracer decomposition method introduced in Banks and Gregory (2006) and Xie and Vallis (2012). Temperature-like tracers denoted as P_1 and P_2 are added to the ocean model in the perturbed experiments to isolate the surface- and circulation-driven ocean temperature anomalies, respectively. Similar to the ocean temperature, the three-dimensional tracer fields are set equal to prescribed temperature values at initialization and are also forced with prescribed surface heat fluxes at each coupling time. The choices of the initial values and surface forcings prescribed for the tracers are determined by the quantity they are designed to isolate. The tracers evolve from their prescribed initial values over time due to their surface forcing and transport by the ocean transport processes. Like the ocean temperature, a tendency equation is also solved in the ocean model to compute the evolution of the tracer fields (see Appendix B of GR20 and the references therein for the description of the tracer equations and the methodology). However, unlike the ocean temperature, the tracers are passive in the sense that they do not affect the ocean density and circulation changes.

Tracer P_1 is designed to emulate the surface-driven anomalous ocean temperature evolution described by (9) (i.e., $P_1 = T'_{OQ}$), while tracer P_2 is designed to emulate the baseline ocean temperature ($\overline{T}_O$) described by (7). However, unlike $\overline{T}_O$, P_2 evolves in a perturbed experiment and is subject to a different ocean transport strength ($v = \overline{v} + v'$). As a result, tracer P_2 evolves differently from $\overline{T}_O$ over time; it can be shown that the difference between the tendency equations for P_2 and $\overline{T}_O$ is equal to the circulation-driven anomalous ocean temperature Equation 10 (i.e., $P_2 = \overline{T}_O + T'_{OO}$). The two tracers thus sum up to the ocean temperature (i.e., $T_O = \overline{T}_O + T'_{OQ} + T'_{OO} = P_1 + P_2$). See Appendix A1 for the description of the initialization and surface forcing for each tracer. Note that in forcing the tracers, F_{OI}, which is included in the CESM surface heat flux output variable, is also removed in order to obtain the provisional surface-driven temperature component.

2.2.3. Frazil and Ocean-Ice Heat Decomposition

The main goal of this study is to decompose the anomalous frazil/ocean-ice heat (F_i/F_{OI}) into components that are driven by anomalous surface heat fluxes and ocean circulation changes. This decomposition is derived from the provisional ocean temperature decomposition described in section 2.2.2 since it isolates ocean temperature changes that cause frazil and ocean-ice heat flux changes through the anomalous surface heat flux and ocean circulation (recall Equation 4). By design, the provisional ocean temperature consists of two parts, represented by the two tracers (recall $T_O = P_1 + P_2$). Similarly, the frazil and ocean-ice heat

energy produced by the provisional ocean temperature can be written as a sum of two parts, contributed by each tracer, that is, $F_i = F_{i_1} + F_{i_2}$ and $F_{OI} = F_{OI_1} + F_{OI_2}$, where F_{i_1}/F_{OI_1} and F_{i_2}/F_{OI_2} are the frazil/ocean-ice heat flux components due to tracers P_1 and P_2, respectively.

F_{i_1}/F_{OI_1} and F_{i_2}/F_{OI_2} are obtained as the weighted contributions of P_1 and P_2 to F_i/F_{OI}, respectively, when P_1 and P_2 are of the "same" sign (e.g., $F_{OI_1} = F_{OI}*P_1/(P_1 + P_2)$). However, P_1 and P_2 sometimes have "opposite" signs, such that a weighting is not appropriate. The freezing temperature is close to zero and the frazil/ocean-ice heat depends most times on the sign of the ocean temperature, such that the ocean temperature components with opposite signs cannot both contribute to the ocean-ice heat flux—only one component can contribute. This can be particularly true in the polar regions in the winter and summer seasons when surface heat fluxes and ocean heat convergence are the opposite. For example, in winter/summer, the ocean over the polar regions loses/gains heat at the surface but gains/loses heat through heat convergence by ocean circulation, so that frazil ice growth/ice melt in winter/summer is primarily caused by the surface heat loss/gain rather than by ocean heat convergence.

Therefore, there are three possible ways to decompose F_i/F_{OI}, when the provisional ocean temperature components are of opposite signs: (1) When $T_O < T_{frz}$ (recall $T_{frz} = -1.8°C$), frazil heat can only be contributed by the tracer component with the negative sign. (2) When $T_O > T_{frz}$ and $T_O > 0$, the ocean-ice heat flux can only be contributed by tracer component with the positive sign. (3) When $T_O > T_{frz}$ and $T_O \leq 0$, the ocean-ice heat flux would also be contributed by tracer component with the positive sign. Though T_O is negative or zero in this case, melt would occur because the provisional ocean temperature has increased from its previous value, that is, the freezing temperature where ice is present. F_{OI} should thus be assigned to the ocean temperature component with the positive sign. In summary, the frazil/ocean-ice heat fluxes are decomposed as follows:

- When P_1 and P_2 are of the same signs; $F_{i_1} = F_i*(P_1/(P_1 + P_2))$ and $F_{i_2} = F_i*(P_2/(P_1 + P_2))$; $F_{OI_1} = F_{OI}*(P_1/(P_1 + P_2))$ and $F_{OI_2} = F_{OI}*(P_2/(P_1 + P_2))$;
- When P_1 and the P_2 are of opposite signs; and

  - $F_i > 0$ and $T_{frz} > T_O$

    * when $P_1 < 0$ and $P_2 \geq 0$; $F_{i_1} = F_i$ and $F_{i_2} = 0$
    * when $P_1 \geq 0$ and $P_2 < 0$; $F_{i_1} = 0$ and $F_{i_2} = F_i$

  - $F_{OI} < 0$ and $T_{frz} < T_O > 0$

    * when $P_1 \leq 0$ and $P_2 > 0$; $F_{OI_1} = 0$ and $F_{OI_2} = F_{OI}$
    * when $P_1 > 0$ and $P_2 \leq 0$; $F_{OI_1} = F_{OI}$ and $F_{OI_2} = 0$

  - $F_{OI} < 0$ and $T_{frz} < T_O \leq 0$

    * when $P_1 \leq 0$ and $P_2 > 0$; $F_{OI_1} = 0$ and $F_{OI_2} = F_{OI}$
    * when $P_1 > 0$ and $P_2 \leq 0$; $F_{OI_1} = F_{OI}$ and $F_{OI_2} = 0$

Similar to the derivation of the surface- and circulation-driven anomalous ocean temperature components with the tracers (i.e., $P_1 = T'_{OQ}$ and $P_2 = \overline{T} + T'_{OO}$), the surface- and circulation-driven frazil/ocean-ice heat flux components are obtained from their tracer-decomposed components as follows: $F_{i_1} = F'_{iQ}$ and $F_{i_2} = \overline{F}_i + F'_{iO}$; $F_{OI_1} = F'_{OIQ}$ and $F_{OI_2} = \overline{F}_{OI} + F'_{OIO}$; so that $F_i = F_{i_1} + F_{i_2} = \overline{F}_i + F'_{iQ} + F'_{iO}$ and $F_{OI} = F_{OI_1} + F_{OI_2} = \overline{F}_{OI} + F'_{OIQ} + F'_{OIO}$. Since frazil heat and ocean-ice heat fluxes in the baseline state are primarily produced by surface heat loss and gain in the winter and summer seasons, respectively, surface-driven anomalous frazil or ocean-ice heat fluxes (F'_{iQ}/F'_{OIQ}) also produced anomalous surface heat loss or gain in the perturbed experiments. However, circulation-driven anomalous frazil or ocean-ice heat fluxes (F'_{iO}/F'_{OIO}) may not result directly from the anomalous ocean heat convergence in the winter and summer seasons, as these warm and cool the polar oceans respectively in these seasons. The circulation-driven frazil and

ocean-ice heat flux anomalies in the winter and summer seasons should instead be viewed as the change in frazil or ocean-ice heat fluxes that occurs if surface heat fluxes are fixed at the baseline values but ocean heat convergence changes (i.e., $F_{iO} = F_{i_2} - \overline{F}_i$).

After F_{i_1}/F_{OI_1} and F_{i_2}/F_{OI_2} are computed, the provisional tracer temperature values are also adjusted with the respective amounts they contribute to the net frazil/ocean-ice heat fluxes. The final and adjusted anomalous ocean temperature components can also be described by the following tendency equations:

$$\frac{\partial T'_{OQ}}{\partial t} = Q' + F'_{OIQ} + F'_{iQ} - v \cdot \nabla T'_{OQ}, \tag{11}$$

and

$$\frac{\partial T'_{OO}}{\partial t} = F'_{OIO} + F'_{iO} - v' \cdot \nabla \overline{T}_O - v \cdot \nabla T'_{OO}. \tag{12}$$

In practice, the tracer-decomposed frazil/ocean-ice heat flux components, F_{i_1}/F_{OI_1} and F_{i_2}/F_{OI_2}, are computed online along with the tracers P_1 and P_2 in the ocean model simulation. Following the same procedure for the ocean temperature and frazil/ocean-ice heat computation in the CESM coupled mode (see section 2.2.1), frazil heat (F_i) is decomposed using the provisional tracer values after F_{IOI} is computed (i.e., where $F_{IOI} > 0$) and within the same coupling time interval the provisional tracer values are computed; the tracers are similarly adjusted after the decomposition of F_i by the amount they each contribute to F_i. On the other hand, the ocean-ice heat fluxes are decomposed in the next coupling time interval, after the actual amount of F_{IOI} used for melt (F_{OI}) is received from the sea ice model. In this case, the tracer values from the previous coupling time interval which have not been adjusted for melt are used to decompose F_{OI}. Each F_{OI} component is then also added to their respective tracer surface flux in the new coupling interval to adjust or reduce the tracer temperature by the amount they contribute to the melt in the previous time step.

The model output of the tracers P_1 and P_2 (ocean model output variables "TTRC_1" and "TTRC_2") and their respective frazil/ocean-ice heat fluxes F_{OI_1} and F_{OI_2} (ocean model output variables "QFLUX1/MELTH_F1" and "QFLUX2/MELTH_F2") are analyzed and compared with total ocean temperature and ocean-ice heat fluxes in section 3.3.1.

2.2.4. The Role of Air-Sea Interactions

The coupling between the atmosphere and ocean further modifies the atmosphere- and ocean-driven sea ice changes. The anomalous surface fluxes and ocean circulation changes that drive ocean-ice heat flux anomalies in a fully coupled experiment are not caused by atmospheric CO_2 increases alone. The ocean circulation response also drives additional anomalous fluxes which can in turn drive additional ocean circulation changes. This two-way interaction makes it difficult to isolate the roles of the atmosphere and the ocean in fully coupled interaction. To isolate the impact of this two-way coupling between the atmosphere and ocean on the sea ice change process, the partial coupling method described in GR20 is used.

The basic idea of this approach is to remove the impact of ocean circulation changes from the air-sea interaction in a partially coupled experiment, such that the anomalous surface fluxes and ocean circulation response are driven by the atmospheric perturbation alone (in this case, CO_2 increase). The partially coupled experiment thus serves the same purpose as a slab ocean experiment, wherein an atmosphere model is coupled with an ocean mixed layer with prescribed ocean heat convergence (Bitz et al., 2012), that is, to exclude the impact of the ocean circulation response from air-sea interaction. However, the partially coupled experiment uses a full dynamical ocean model and thereby can simulate an ocean circulation response but without the impact of coupling and also allow for changes in ocean mixed layer thickness and ocean transport of anomalous surface heat fluxes that are not simulated in slab ocean experiments. When compared with the sea ice response in a fully coupled experiment, the partially coupled experiment can thus show how atmosphere-ocean coupling modifies the sea ice loss process through its impact on both anomalous surface heat fluxes and ocean circulation changes.

Table 1
Tracer Configurations and Their Use in the Partially and Fully Coupled Simulations for Decomposing the Frazil Heat (F_i) and Ocean-Ice Heat Fluxes (F_{OI})

Experiment	Tracer	Initialization	Temperature equivalence	Frazil heat and ocean-ice heat equivalence
Fully coupled	P_1	$P_1\|_{t=0} = 0$	$P_1 = T'_{OQ}$	$F_{i_1} = F'_{iQ}\ F_{OI_1} = F'_{OIQ}$
	P_2	$P_2\|_{t=0} = \overline{T}_O;$	$P_2 = \overline{T}_O + T'_{OO}$	$F_{i_2} = \overline{F}_i + F'_{iO}\ F_{OI_2} = \overline{F}_{OI} + F'_{OIO}$
Partially coupled	P_1	$P_1\|_{t=0} = 0$	$P_1 = T'_{OQ_A}$	$F_{i_1} = F'_{iQ_A}\ F_{OI_1} = F'_{OIQ_A}$
	P_2	$P_2\|_{t=0} = \overline{T}_O$	$P_2 = \overline{T}_O + T'_{OO_P}$	$F_{i_2} = \overline{F}_i + F'_{iO_P}\ F_{OI_2} = \overline{F}_{OI} + F'_{OIO_P}$

Note. Q' indicates the anomalous air-sea heat fluxes in the fully coupled experiment, and QA' indicates the atmosphere-driven ones in the partially coupled experiment. Tracer P_1 isolates the surface-driven anomalous ocean temperature components (T'_{OQ} and T'_{OQ_A}) forced by Q' and QA', while tracer P_2 isolates the baseline ($\overline{T}_O$) and circulation-driven anomalous components (T'_{OO} and T'_{OO_P}) forced by the circulation changes v' and vp' in the fully and partially coupled experiment. F_{i_1}/F_{OI_1} are the frazil heat and ocean-ice heat flux components due to P_1, while F_{i_2}/F_{OI_2} are the ones due to P_2.

The fully and partially coupled experiments are initialized from the same point in the control experiment and also forced with CO_2 quadrupling. Tracers P_1 and P_2 are also added to both experiments to decompose their respective anomalous ocean temperature and frazil/ocean-ice heat fluxes into the surface- and circulation-driven components as described above. However, unlike the fully coupled experiment where the actual ocean surface temperature is used to compute surface flux exchange in the coupler (i.e., $T_{cpl} = T_O = \overline{T}_O + T'_{OQ} + T'_{OO}$), a surrogate ocean temperature that includes the baseline and only the surface-driven anomalous component is used in the partially coupled experiment (i.e., $T_{cpl} = \overline{T}_O + T'_{OQ_A}$) so that the circulation-driven component (T'_{OO_P}; see Table 1) is removed from the air-sea interaction. $\overline{T}_O$ (from the control experiment) is supplied as input so that similar baseline surface heat fluxes ($\overline{Q}$) are simulated in the partially coupled experiment as the fully coupled one. As a result, only atmosphere-driven anomalous surface heat fluxes (Q'_A) are simulated in the partially coupled experiment, while the anomalous surface heat fluxes (Q') in the fully coupled experiment include both atmosphere- and ocean-driven components (i.e., $Q' = Q'_A + Q'_O$) due to the additional circulation-driven ocean temperature component (T'_{OO}) that is coupled. Similar to the one in the fully coupled experiment, tracer P_1 isolates the surface-driven ocean temperature anomalies in the partially coupled experiment so that the surrogate ocean temperature coupled with the atmosphere in this experiment is equal to $\overline{T}_O + P_1\|_s$ (see GR20 for full description and validation of partially coupled experiment and tracer equations).

It is important to note that only the atmosphere-ocean coupling is partial in this experiment, and the sea ice model is fully coupled with both atmosphere and ocean models. In both the fully and partially coupled experiments, frazil ice growth and bottom melt rates are primarily computed with freezing/melting potential (F_{IOI}) in the sea ice model, and F_{IOI} is computed using the actual ocean temperature (i.e., T_O). Using the actual ocean temperature for computing F_{IOI} is necessary for the ocean temperature to be fully adjusted for freezing and to prevent it from dropping unrealistically below the freezing temperature. It is also possible that a partial ocean temperature be used for computing the F_{IOI}, but the actual ocean temperature is adjusted for freezing; however, this would not allow energy conservation in the ocean model. Nevertheless, the partial atmosphere-ocean coupling has an indirect impact on the frazil/ocean-ice heat fluxes. Because the anomalous surface fluxes and ocean circulation changes simulated in the partially and fully coupled experiments are different, their ocean temperatures and the resulting frazil/ocean-ice heat fluxes and sea ice responses are also different. A comparison of the sea ice volume budget and the surface- and circulation-driven frazil/ocean-ice heat flux components in the fully coupled and partially coupled experiments thus isolates how atmosphere-ocean coupling alters the sea ice loss process.

We further checked that the partial coupling does not introduce a drift or spurious surface heat flux changes by conducting another (20-year-long) baseline experiment using the same partial coupling as the perturbed partially coupled experiment but without CO_2 quadrupling. Comparing this partially coupled control run to the original fully coupled control experiment indicated that the impact of partial coupling on global averaged anomalous surface heat gain and ocean temperature is indeed negligible (see Figures S1 and S2 of GR20). Arctic sea ice is about 20% thicker in the partially coupled baseline than the fully coupled one, but sea ice
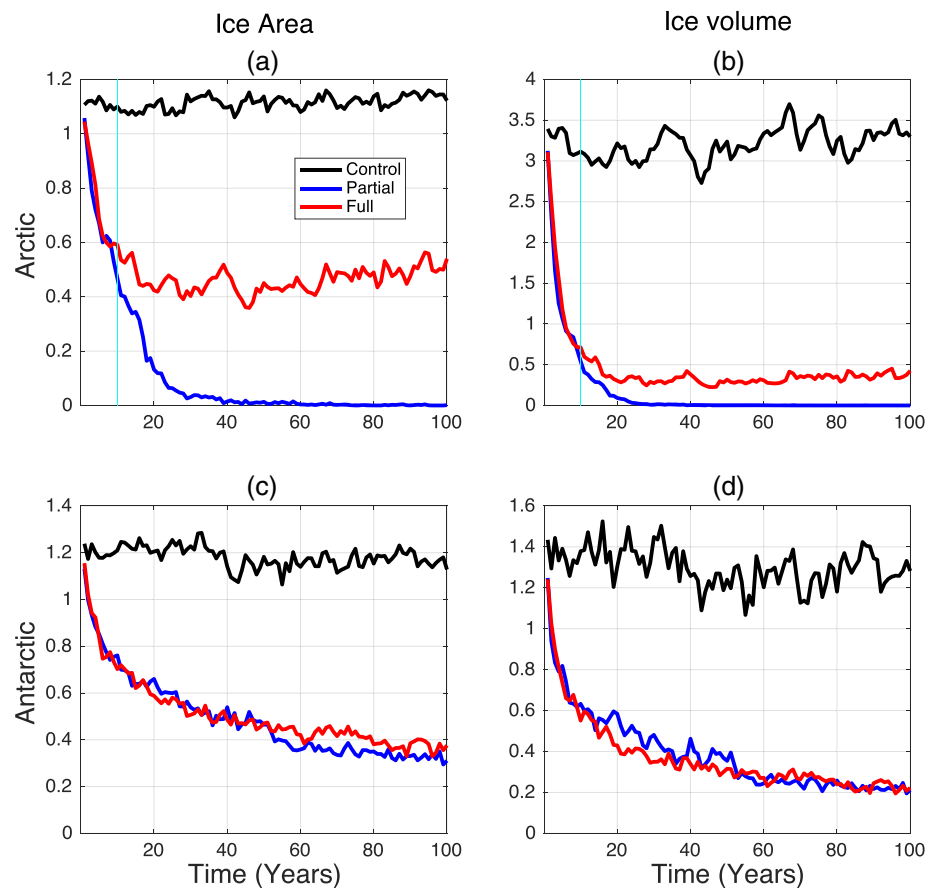
Figure 1. Annually integrated sea ice area (in $10^7 \, km^2$) and volume (in $10^4 \, km^3$) in the Arctic (a, b) and Antarctic(c, d) for the preindustrial control (black) and fully coupled (red) and partially coupled (blue) perturbed experiments. The standard deviations of Arctic sea ice area and volume are respectively $0.02 \times 10^7 \, km^2$ and $0.18 \times 10^4 \, km^3$ and $0.04 \times 10^7 \, km^2$ and $0.09 \times 10^4 km^3$ for the Antarctic. Cyan line shows the 10-year period of rapid Arctic sea ice loss.

extent is very similar. Interannual variability in Antarctic ice extent and volume is also similar in the two runs, but phases of internal interannual oscillations differ (Figures S1 and S2 in the supporting information). Changes evident when comparing the perturbed (fully and partially coupled) experiments after CO_2 are quadrupled are much larger than the unperturbed variants indicating that the differing response in the fully and partially coupled frameworks is a robust response to the coupling strategy in the presence of forcing. As we will see, the differences in the sea ice response of the partially and fully coupled perturbed experiment are related to the different rates of decrease of their sea ice extent in winter, which are very similar in the baseline experiments; thus, the conclusions are robust despite differences in the baseline.

3. Results

3.1. Arctic Sea Ice Volume Change and its Budget

The sea ice area and volume evolution in the perturbed fully coupled and partially coupled experiments are shown in Figures 1–3. Arctic sea ice volume decreases more rapidly than that of the Antarctic in both experiments (Figures 1b and 1d). More significantly, Arctic sea ice area and volume evolve differently in the fully and partially coupled experiments (Figures 1a, 1b, 2, and 3), while Antarctic sea ice evolves similarly in the two experiments (Figures 1c and 1d; also compare Figures S3 and S4).

In the first 10 years following abrupt CO_2 quadrupling, Arctic sea ice area and volume decline at similar rates in the fully and partially coupled experiments (Figures 1a and 1b). This initial period accounts for most of the Arctic's sea ice thickness or volume loss, about two thirds of the sea ice volume loss in the fully coupled
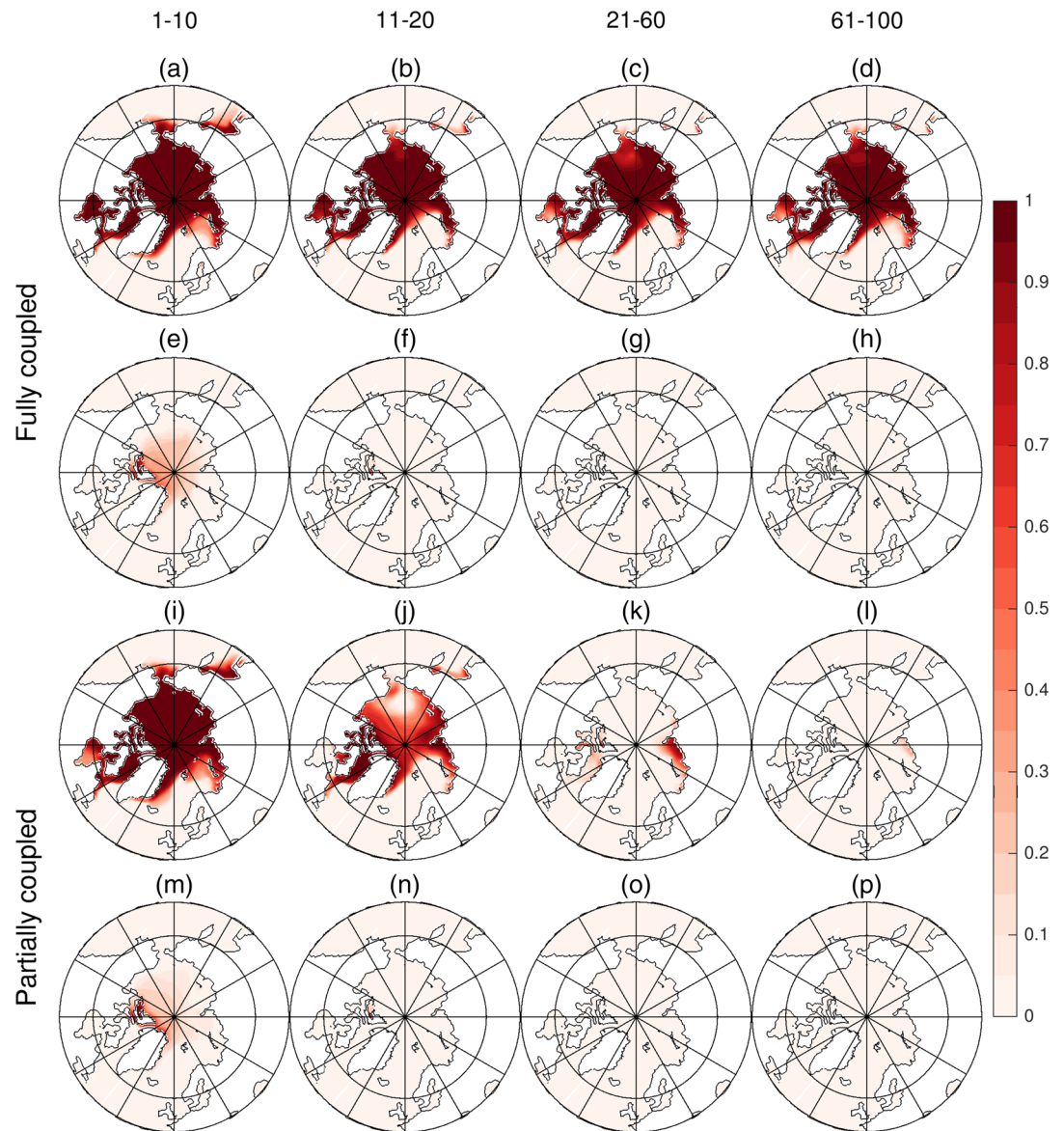
Figure 2. Time-averaged Arctic March and September sea ice concentration in the fully (a–h) and partially coupled experiments (i–p) for Years 1–10 (a, e, i, m), 11–20 (b, f, j, n), 21–60 (c, g, k, o), and 61–100 (d, h, l, p).

experiment. Following the initial phase of rapid ice loss, Arctic sea ice area and volume continues to decline but do so more slowly and at different rates in the fully and partially coupled experiments (Figures 1a and 1b). By the end of 20 years, the Arctic becomes seasonally ice free in both experiments (Figures 2 and 3 [panels b, f, j, and n]). However, in the partially coupled experiment, the sea ice decline continues after 20 years so that the Arctic becomes completely ice free in all seasons by the end of 40 years (compare Figures 1a and 1b and Figures 2 and 3 [panels k, l, o, and p]). While in the fully coupled experiment, the sea ice loss stabilizes after 20 years, and though the Arctic remains seasonally ice free, it continues to grow ice in winter (Figures 2 and 3 [panels c, d, g, and h]; compare also Figure S6). In the Antarctic, the seasonal sea ice changes are much more alike in both experiments throughout the 100-year simulation (compare Figures S3 and S4).

These differing Arctic sea ice responses in the fully and partially coupled experiments suggest that the impact of ocean circulation changes on the air-sea interactions play a stabilizing role in maintaining
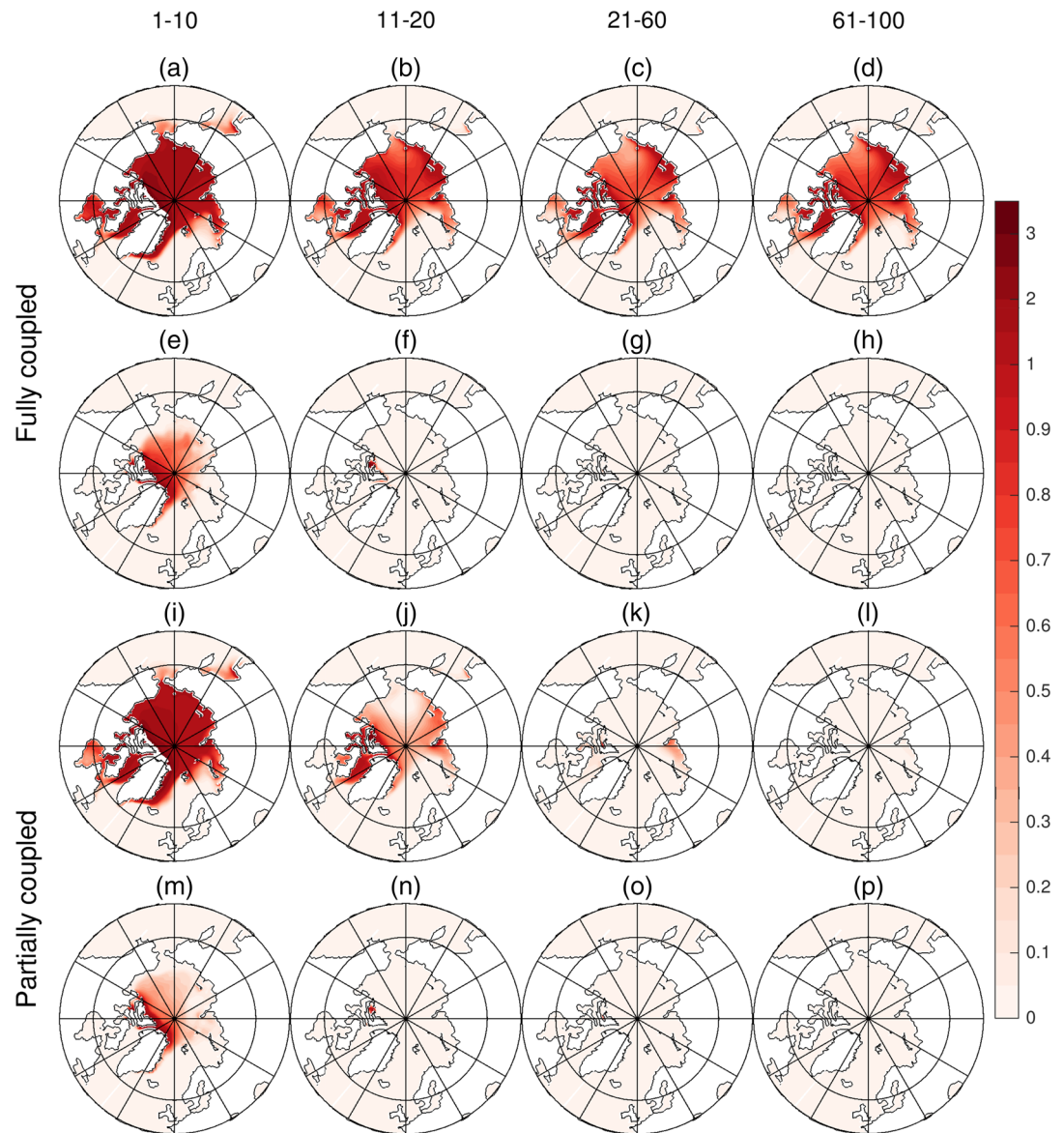
Figure 3. Time-averaged Arctic March and September sea ice thickness in the fully (a–h) and partially coupled experiment (i–p) for Years 1–10 (a, e, i, m), 11–20 (b, f, j, n), 21–60 (c, g, k, o), and 61–100 (d, h, l, p). Units = m.

seasonal sea ice in the Arctic, while this impact is not significant in the Antarctic. To understand the roles of the atmosphere and ocean and the coupling between them in Arctic sea ice response and why they differ in the Antarctic, we examine Arctic sea ice volume budget and the role of frazil/ocean-ice heat flux components in both experiments and how they differ in the Arctic and Antarctic in the next sections.

3.1.1. Arctic Sea Ice Volume Budget

We now analyze the Arctic sea ice volume budget in the light of the contributions from the volume changes at sea ice top and bottom interfaces, first in the control and then in the perturbed fully and partially coupled experiments. In order to have a complete sea ice volume budget, we use annual integrals of growth and melt rates (Figure 4); however, these annual growths and melt rate changes largely occur in the winter and summer seasons, respectively (Figures 6, 7, and S6–S8).

In the preindustrial control experiment, stable Arctic sea ice volume is maintained by a balance between a net volume loss at the top face and a net volume gain at the bottom face (Figures 4c, 4f, and 4i, black lines).
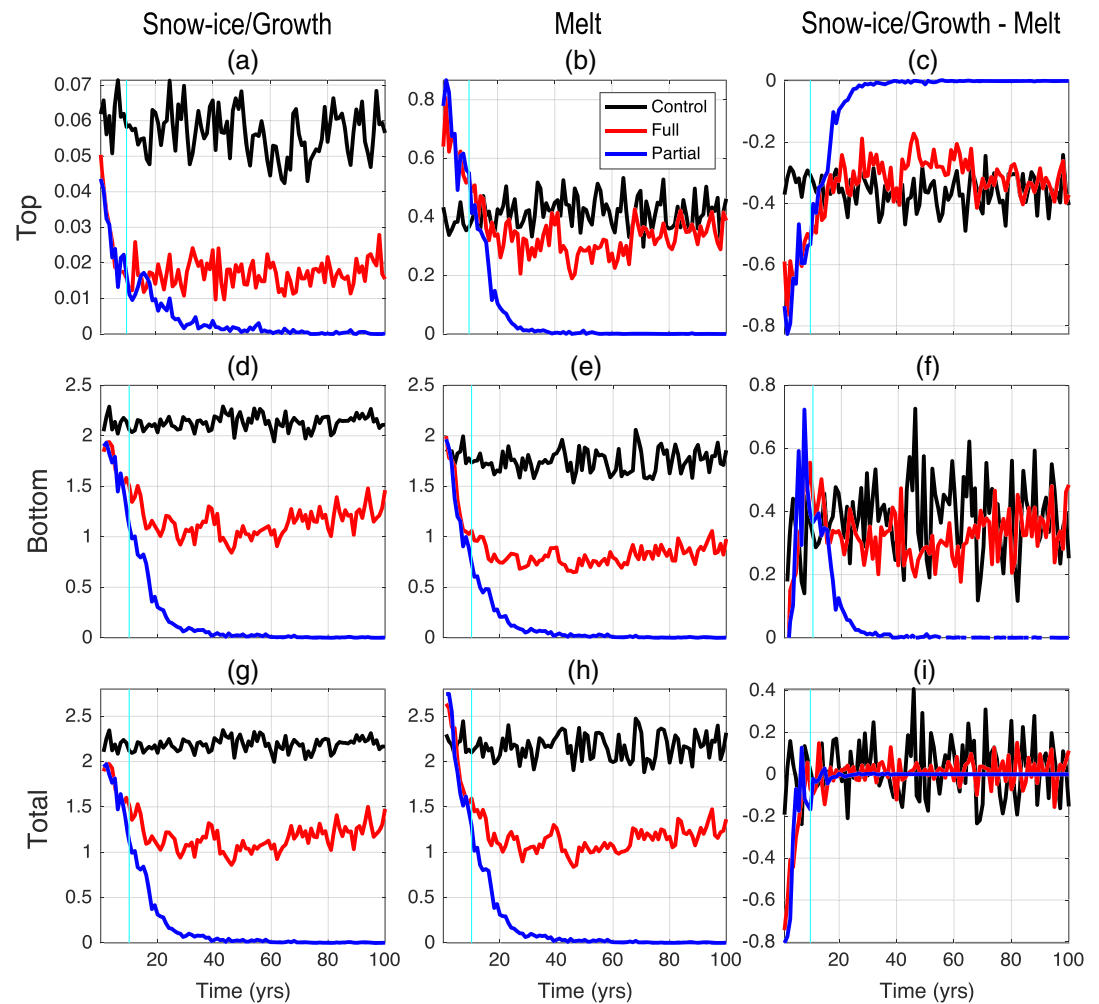
Figure 4. Arctic sea ice volume budget (units $= 10^4$ Km^3/year; note that each panel uses a different range on the y axis to expose the response for that field). Annually integrated sea ice growth, melt, and the net volume change rate (growth-melt) at the sea ice top face (a–c), bottom face (d–f), and total (top + bottom; g–i) in the preindustrial control (black), fully coupled (red), and partially coupled CO_2 quadrupling experiments (blue). Standard deviations for top face melt and growth rates are 0.05 and 0.006×10^4 Km^3/year, respectively, and bottom face melt and growth rates are 0.11 and 0.07×10^4 Km^3/year, respectively. Cyan line shows the 10-year period of rapid Arctic sea ice loss.

Though the net volume loss and gain at the top and bottom faces are equal, the magnitudes of the growth and melt rates at the ice top face are much smaller than those at the bottom face (compare Figures 4a, 4b, 4d, 4e, and S5). That the rate of ice melt at the bottom face exceeds ice melt at the top interface may be attributed to the greater reflectivity of sea ice compared to the surrounding (ice-free) ocean surface (Bitz et al., 2005). Net volume loss at the top face occurs because Arctic sea ice grows very little by snow accumulation in winter but melts vigorously at its top face in summer (growth < melt; Figures 4a and 4b, black lines; compare Figures S5a–S5c), while at the ice bottom face, net volume gain occurs because winter bottom growth exceeds summer melt (growth > melt; Figures 4d and 4e, black lines; compare Figures S5g–S5i).

With CO_2 quadrupling, the initial phase of a similar rapid decrease in Arctic sea ice volume in both fully and partially coupled experiments (first 10 years; recall Figure 1) occurs largely due to an increase in the volume loss at the ice top face (Figure 4c, red and blue lines). This increase in the top face volume loss is caused by an increase in the top melt rate in summer; the top face growth rate is much smaller in comparison (Figures 4a–4c, red and blue lines). Volume gain at the ice bottom face also decreases initially but quickly recovers
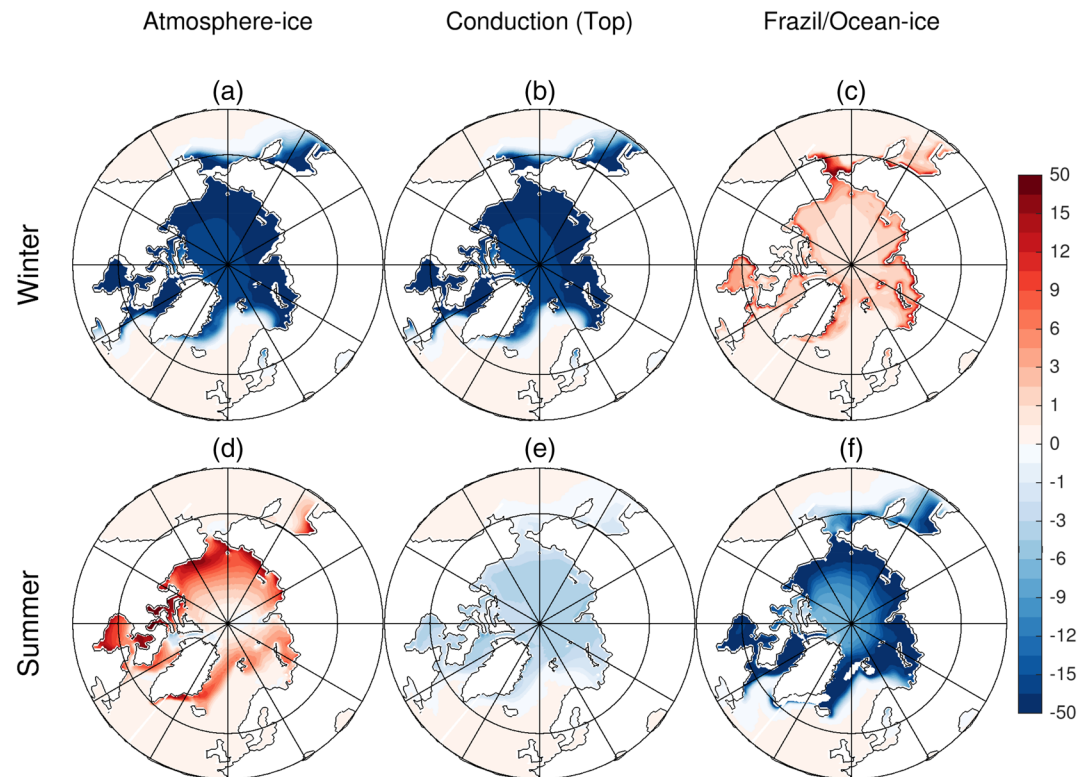
Figure 5. Time-averaged baseline atmosphere-ice heat fluxes, F_{AI}, conductive fluxes through the ice at the top face, $k\partial T_I/\partial z$, and ocean-ice heat fluxes, F_{OI}, in the winter (DJFM; a–c) and summer (MJJA; d–f) seasons, respectively, in the preindustrial control experiment. Note that sign convention for atmosphere- and ocean-ice heat fluxes are positive downward; units: W/m^2.

and so does not contribute much to the overall Arctic volume loss during this period (Figure 4f, red and blue lines). However, after several years, the ice top face melt rate increase quickly attenuates and eventually becomes weaker than the baseline top face melt rate in the control experiment (Figures 4b and 4c; compare red and blue with black lines). The large decrease in Arctic sea ice volume in the decade following this initial phase of Arctic sea ice loss explains the decrease of the ice top face summer melt rate that occurs despite persistent increases in surface temperatures (Figures 1b, S7, and S8a–S8d).

In the ensuing years (years 10 to 100), Arctic sea ice volume declines at a slower but different rates in both experiments, especially between Years 10 and 20 (recall Figure 1 and Figures 2 and 3 [panels b and j]). This relatively slow period of Arctic sea ice volume loss rate is largely caused by the decrease in the annual net volume gain at the ice bottom face (Figure 4f; compare red and blue with black lines). The Arctic had become seasonally ice free in this period such that the annual net Arctic sea ice volume depends on the net sea ice volume that reappears in winter. The decrease in the annual net sea ice volume thus results from the decrease of the bottom face volume gain in winter (Figures 2 and 3; compare panels a–d with panels e–h and panels i–l with panels m–p).

The decrease in the bottom face volume gain in winter is caused by the decrease in the bottom face growth rates. Bottom face melt rates that largely occur in summer decrease, rather than increase in this period in both fully and partially coupled experiments (Years 10 to 100; Figures 4d and 4e). The decrease in the bottom melt rates in summer is explained by the decrease in the net bottom face sea ice growth that occurred in winter. The decrease of the bottom face growth rate occurs even faster in the partially coupled experiment (Figures 4d and 4f; compare the difference between red and blue lines); this explains why the annual net sea ice volume decreases more rapidly in the partially coupled experiment during this period (compare red and blue lines in Figures 4f, 3a, and 3b). The Arctic volume budget analysis thus indicates that Arctic sea ice loss is initially (1–10 years) driven by an increase in its top face melt rates in summer and then later (10–100 years) by a decrease in the bottom growth melt rates in winter.
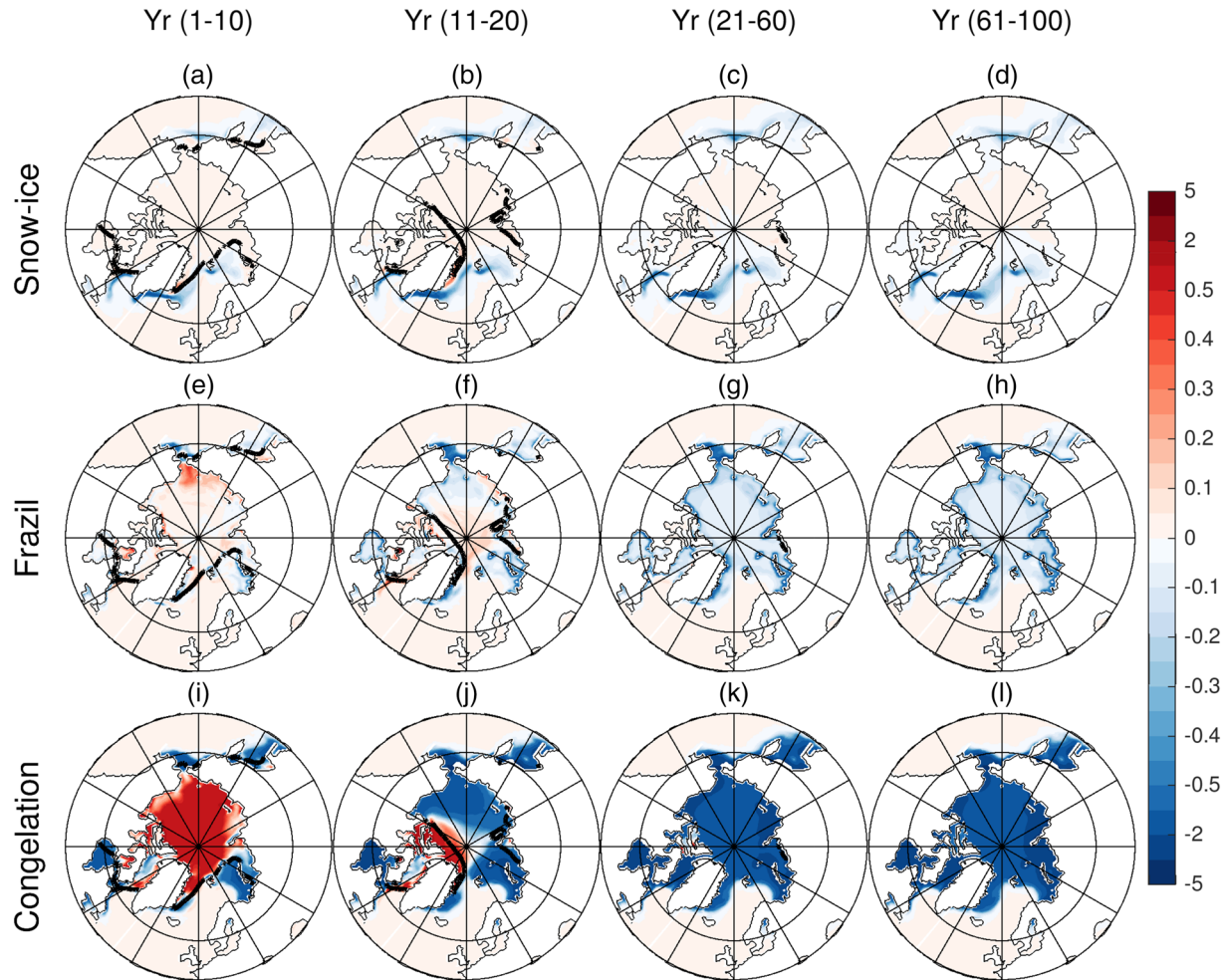
Figure 6. Time-averaged Arctic winter (JFMA) sea ice growth components; snow-ice formation (a–d), frazil (e–h), and basal (i–l) growth anomalies for Years 1–10 (a, e, i), 11–20 (b, f, j), 21–60 (c, g, k), and 61–100 (d, h, l) in the partially coupled experiment. Unit = m/year. Solid dark lines show the time-averaged sea ice extent.

3.2. Attribution of Sea Ice Volume Changes to Atmosphere-Ice and Frazil/Ocean-Ice Heat Changes

In order to isolate the roles of the anomalous atmosphere-ice and frazil/ocean-ice heat fluxes in the sea ice volume changes described above, it is necessary to understand how atmosphere-ice and frazil/ocean-ice heat fluxes drive sea ice growth and melt rates seasonally in the baseline state. Following Equations 1 to 3, changes in growth and melt rates at the sea ice top and bottom faces cannot simply be attributed to the atmosphere- and frazil/ocean-ice heat fluxes due to the presence of the conductive term ($k\partial T_I/\partial z$ in Equations 1 and 2). Understanding how heat conduction at the sea ice interfaces varies seasonally is thus useful for attributing the roles of the atmosphere- and frazil/ocean-ice heat fluxes.

Heat conduction through sea ice is a function of the temperature difference between the top and bottom faces. Sea ice temperature itself must be at or below T_{frz} (otherwise, it melts), and sea ice temperature at the ocean-ice interface must be maintained at the freezing temperature (sea ice grows or melts when the ocean temperature falls below or rises above freezing) so that the vertical gradient of temperature between the sea ice top and the base is often negative, and heat conduction through sea ice is often upward.

In summer, melting at the sea ice interfaces occur at similar constant temperatures so that the vertical gradient of sea ice temperature and heat conduction between ice interfaces are small (i.e., $k\partial T_I/\partial z \approx 0$ (Figure 5e); $-q\partial h/\partial t|_{top} \approx F_{AI}$ in (1); $q\partial h/\partial t|_{bot} \approx F_{OI_b}$ in (2)). Summer melt rates at sea ice top and bottom faces are thus largely attributable to atmosphere-ice and ocean-ice heat fluxes, respectively (compare
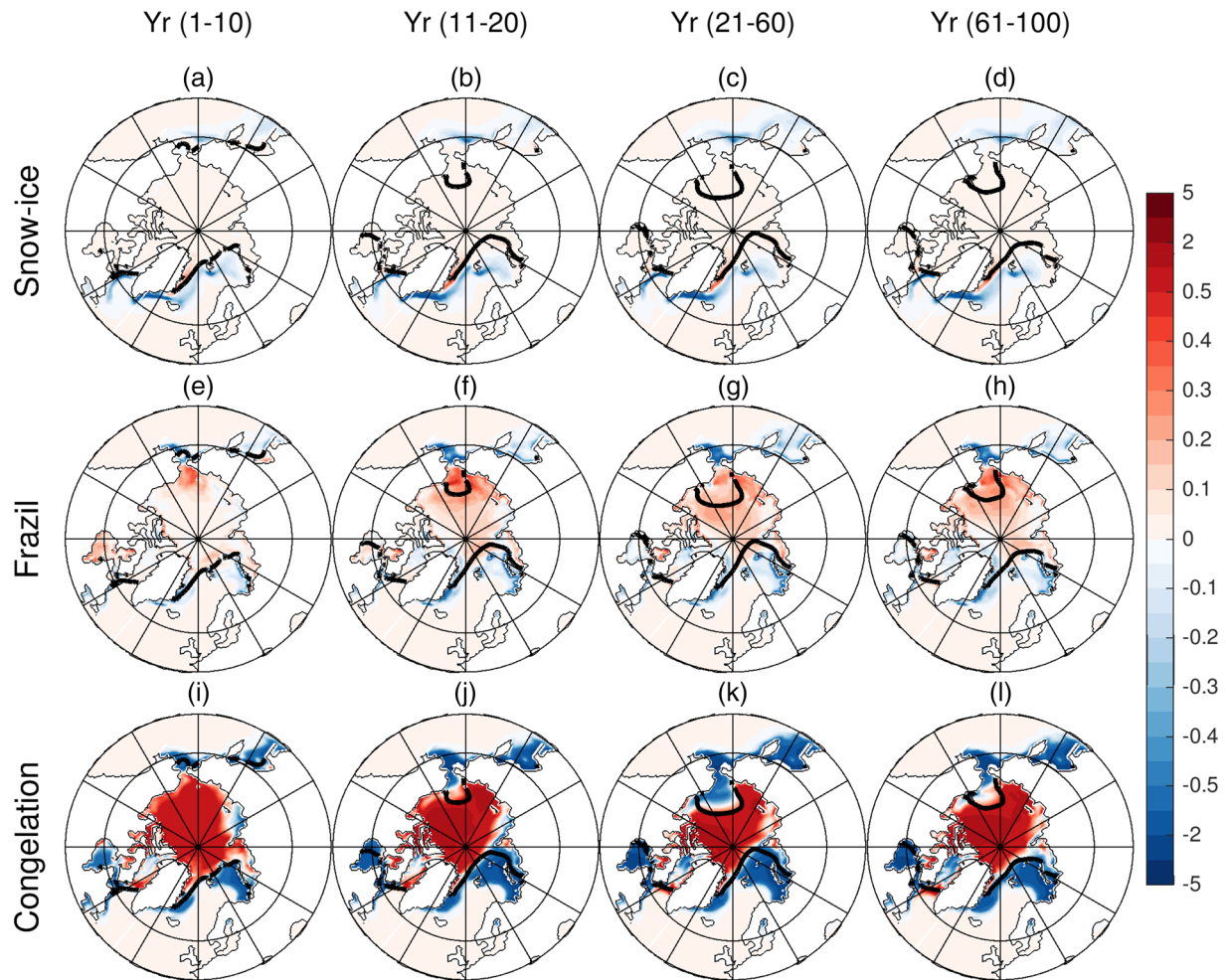
Figure 7. Same as Figure 6 but for the fully coupled experiment.

atmosphere- and ocean-ice heat fluxes [Figures 5d and 5f] with summer melt rates [Figures S5b and S5h]). On the other hand, in the winter season, sea ice growth cannot occur at the top face, and the atmosphere-ice heat fluxes are largely used for cooling sea ice temperature; some fraction of the atmosphere-ice heat fluxes can be used for snow-ice conversion when snow is available (i.e., $\partial h/\partial t|_{top} \approx 0$ [Figure 5a]; $I_O \approx 0$ in winter and $F_{AI} \approx k\partial T_I/\partial z$ in (1); compare Figures 5a and 5b). Since the bottom face is constantly maintained at the freezing temperature, the cooling of sea ice temperature by atmosphere-ice heat fluxes causes a large vertical gradient of sea ice temperature, which drives basal ice growth at the bottom face by conduction ($k\partial T_I/\partial z$ in Equation 2; compare Figures 5a, 5b, and S5g). On the other hand, frazil heat is used for frazil ice formation where the ocean temperature falls below freezing (Equation 3; compare Figures 5c and S5d).

Basal ice growth accounts for most of the sea ice growth in winter, with frazil ice formation making a much smaller contribution (Figures S5d and S5g). However, despite its much smaller contribution, frazil ice growth still plays a crucial role in the net sea ice growth in winter. Basal sea ice growth can *only* occur below existing ice, so its net amount depends on sea ice extent. Sea ice extent at the beginning of the winter season is greatly reduced by the preceding summer melt (summer basal melt > winter basal growth around the sea ice edges; Figure S5i). Therefore, the net amount of sea ice growth in winter also depends on the seasonal increase in sea ice extent by frazil ice formation. The net sea ice growth in winter thus depends on both atmosphere and frazil heat fluxes.

Similarly, in the perturbed experiments, conduction is even weaker in summer (compare Figure 5e with anomalies in Figures S10 and S11e–S11h) so that the initial anomalous increase of the melt rates at the ice top face in summer can be attributed to the anomalous increase in atmosphere-ice heat fluxes in the
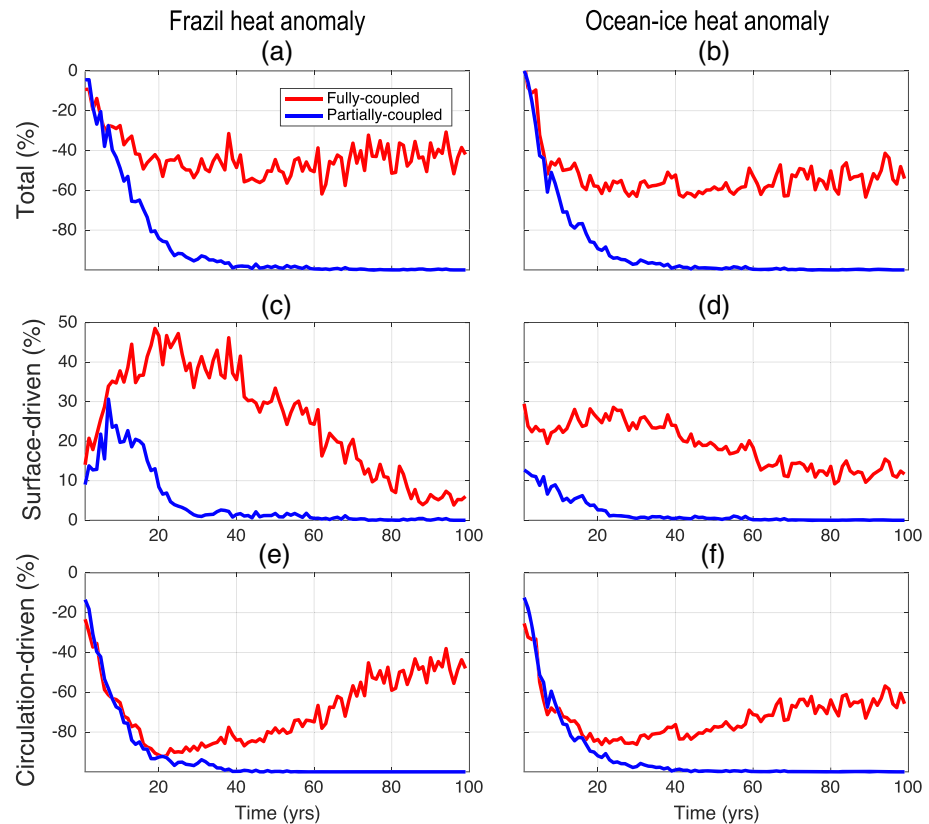
Figure 8. Percentage anomalies of the annually integrated Arctic frazil and ocean-ice heat fluxes (a, b) and their surface-driven (c, d) and circulation-driven (e, f) components in the fully coupled (red) and partially coupled (blue) simulations. Percentage anomalies are taken with respect to the annually averaged frazil and ocean-ice heat fluxes in the control experiment. Positive (negative) percentages show anomaly increase (decrease). The coefficients of variation for frazil and ocean-ice heat fluxes in the preindustrial control experiment are 3.8% and 5.73%, respectively.

perturbed experiments (Figures S10 and S11a–S11d). The greater contribution of the anomalous summer melt rates at the ice top face to the sea ice volume loss in the initial phase of rapid Arctic sea ice decline (within the first decade) thus suggests that the atmosphere plays a dominant role in rapid sea ice volume decline in the short term.

On the other hand, the greater role played by the bottom face growth rates in winter in the later phase (beyond 10 years) of Arctic sea ice loss could indicate that slower ocean processes play a greater role in the long term. As in the baseline state, changes in the net winter growth rates in the perturbed experiments could be driven both by changes in atmosphere-ice heat flux changes and frazil ice formation associated with ocean temperature changes. However, because the Arctic becomes seasonally ice free during this period in the perturbed experiments, the role of frazil ice growth becomes even more crucial than in the baseline winter growth process, as frazil ice growth becomes necessary for the reappearance of sea concentration in winter. Basal ice growth and atmosphere-ice heat fluxes actually increase where ice concentration reappears in winter; anomalous basal growth decrease occurs only at the sea ice edges where sea ice concentration has declined (compare Figures 6 and 7 [panels i–l] and S12 and S13 [panels a–d and e–h]). Therefore, the decrease in the net winter ice growth rates after the first decade and its differring rates between the fully and partially experiments, can be attributed to the decrease in net sea ice area available for basal ice growth that result from a decrease in frazil ice growth or frazil heat.

3.3. The Role of Surface Heat Fluxes and Ocean Circulation Changes in the Ocean-Driven Arctic Sea Ice Changes

3.3.1. Anomalous Frazil Heat Components

We next examine the relative contributions of the surface- and circulation-driven components to the frazil heat decrease (i.e., F'_{iQ} and F'_{iO}; see section 2.2.3). These components provide further insight into the
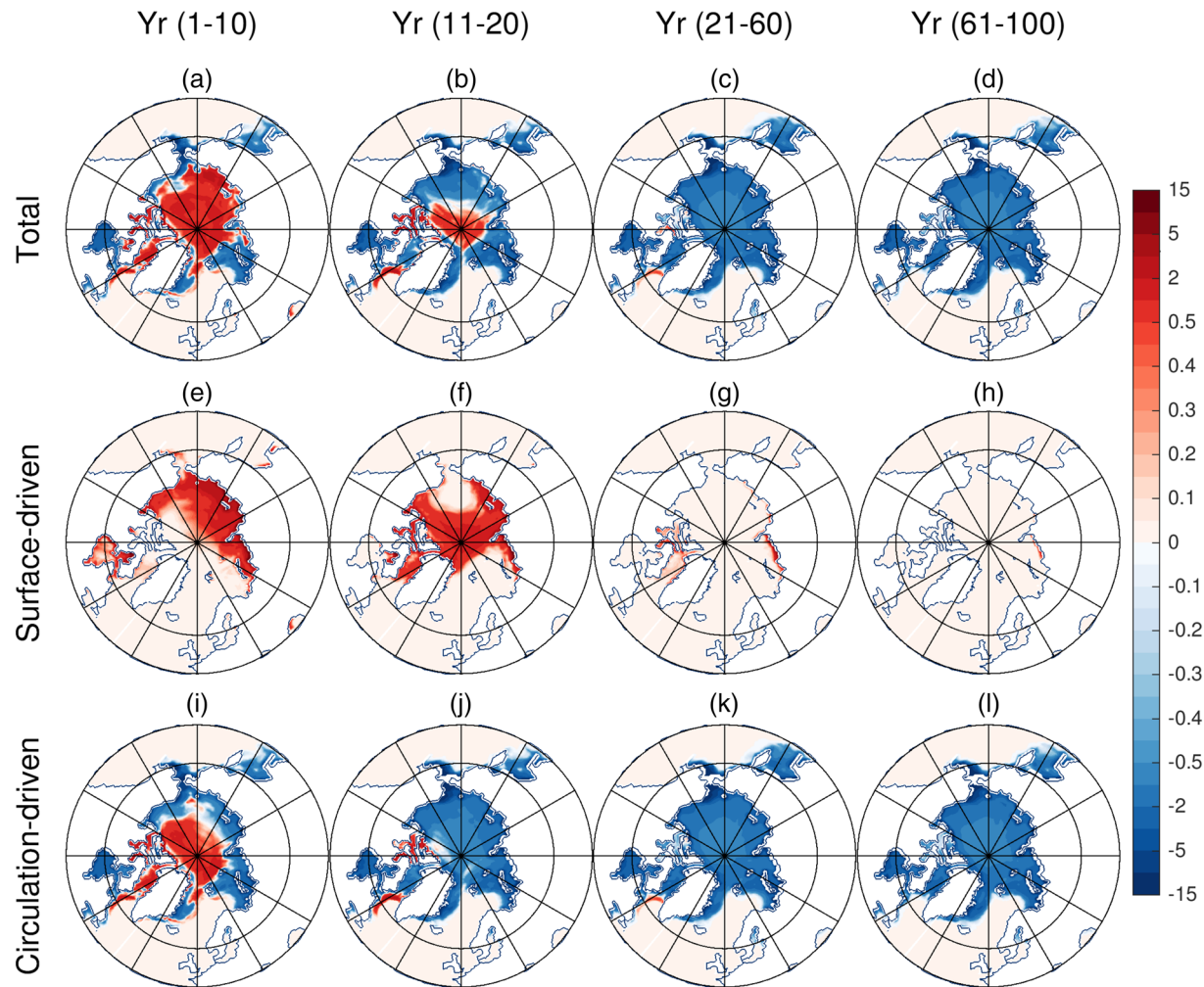
Figure 9. Time mean Arctic winter season (DJFM) frazil heat fluxes (a–d) and their surface-driven (e–h) and circulation-driven (i–l) components for Years 1–10 (a, e, i), 11–20 (b, f, j), 20–60, and 60–100 (d, h, l) in the partially coupled experiment. Unit is W/m^2.

ocean processes that drive the frazil heat changes and the resulting sea ice extent and winter growth decreases, and further isolate the possible impact of the atmosphere on the decrease. The surface-driven component indicates the atmospheric impact on the frazil heat through the anomalous surface heat loss from the ocean, while the circulation-driven changes isolate the impact of the ocean circulation changes only. Note that, though frazil ice growth is primarily caused by the ocean's surface heat loss to the atmosphere in winter, a decrease in frazil ice growth could be caused by both an increase in the ocean heat convergence into the Arctic or a decrease in the Arctic's surface heat loss to the atmosphere. In the remaining discussions, we limit our discussion to the frazil heat components instead of those of the ocean-ice heat fluxes; as we discussed in the preceding section, sea ice volume decrease in this period is driven by the decrease in frazil ice formation. The decrease of the ocean-ice heat fluxes and the resulting ice bottom face melt are also not explained by anomalous ocean temperature (which increase in this period); rather, the decrease is explained by the growth-driven sea ice volume decrease in this period (compare Figures 8b, 8d, and 8f with 8a, 8c, and 8e).

Surface- and circulation-driven anomalous frazil heat components have opposite impacts on the net frazil heat changes. The surface-driven component causes an increase rather than a decrease in frazil heat and also contributes to the smaller percentage of change of the frazil heat anomalies. The circulation-driven component, on the other hand, causes the decrease in frazil heat and contributes to the greater percentage of change of the frazil heat anomalies (compare Figures 8c and 8d with Figures 8e and 8f). The relative contributions of these components suggest that the impact of the atmosphere is indeed small and the ocean drives
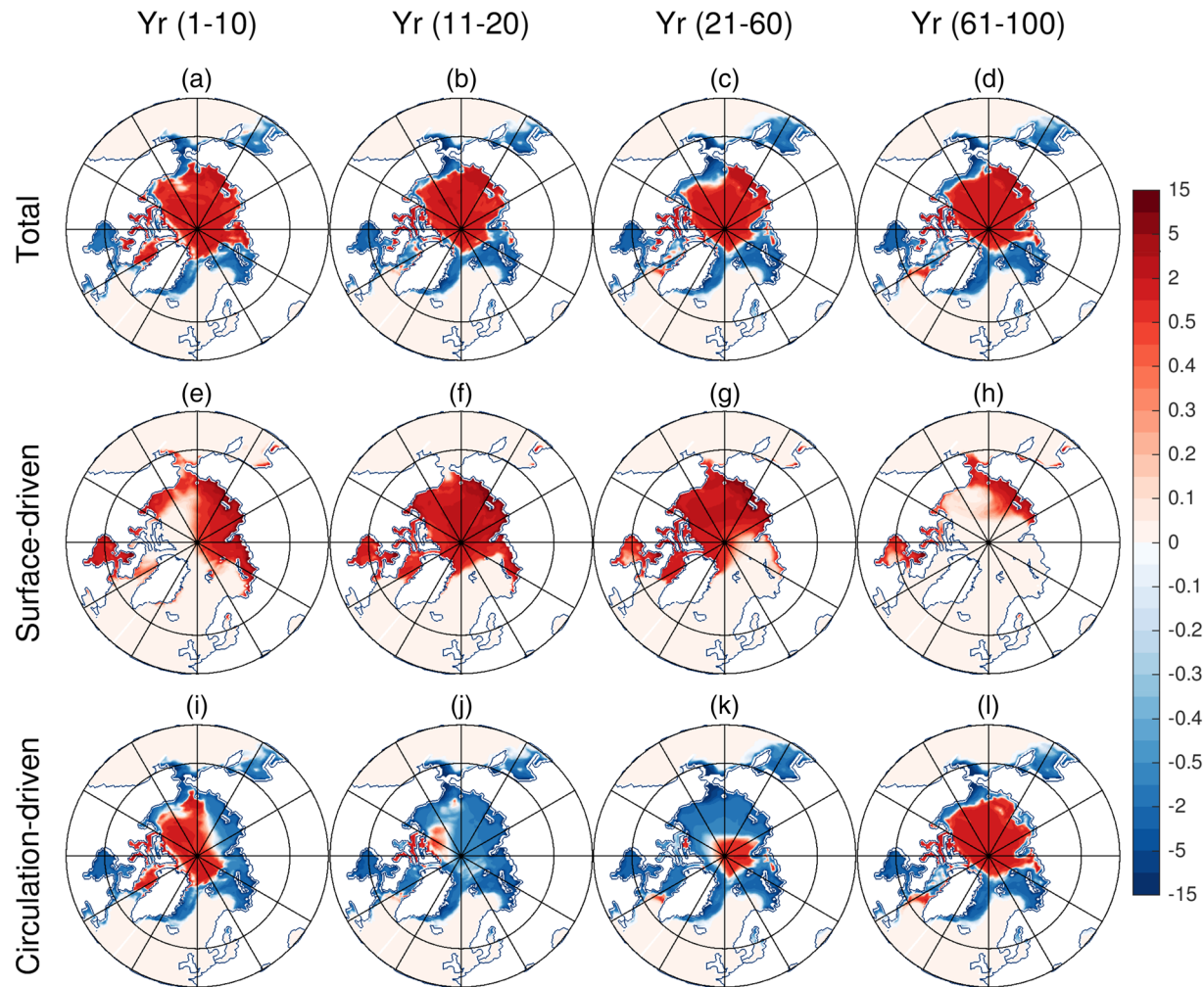
Figure 10. Same as Figure 9 but for the fully coupled experiment.

the decrease of sea ice growth rates in winter. The surface-driven component suggests anomalous surface heat loss from the ocean increase in winter and only acts to slow down the greater circulation-driven decrease of frazil heat. This anomalous increase in winter surface heat loss in the Arctic likely occurs for the same reason atmosphere-ice heat fluxes or conduction increase where sea ice concentration exists in winter (compare Figures 6 and 7 [panels i–l] and S12 and S13 [panels a–d and e–h]). Surface air temperatures over the Arctic increase a lot more than the ocean surface temperatures or the sea ice top face temperature, thereby increasing the surface sensible heat loss and the resulting surface-driven frazil heat in the Arctic (see also Figure 4e of GR20).

The anomalous frazil heat components further explain the different rates of Arctic sea ice loss after 10 years in the partially and fully coupled experiments (i.e., the bottom-growth-driven period of Arctic sea ice volume loss) and the similar rates of Antarctic sea ice loss in both experiments (recall Figure 1). In the Arctic, a surface-driven increase of frazil heat occur at similar rates up to about 10 years in both experiments. But after 10 years, this surface-driven increase of frazil heat continues in the fully coupled experiment, while it quickly declines in the partially coupled experiment (Figure 8c; compare also Figures 9 and 10 [panels e and f]). On the other hand, the circulation-driven components decrease at similar rates in both experiments up to about 20 years (Figures 8e; compare also Figures 9 and 10 [panels i and j]). Greater surface-driven increase of frazil heat in the fully coupled experiment thus explains the slower decline of the net frazil heat between years 10 and 20 in this experiment (Figure 8a), which, in turn, explains the slower decrease of its sea ice area and bottom growth rates in this period (compare Figures 1 and 4e, red and blue lines).
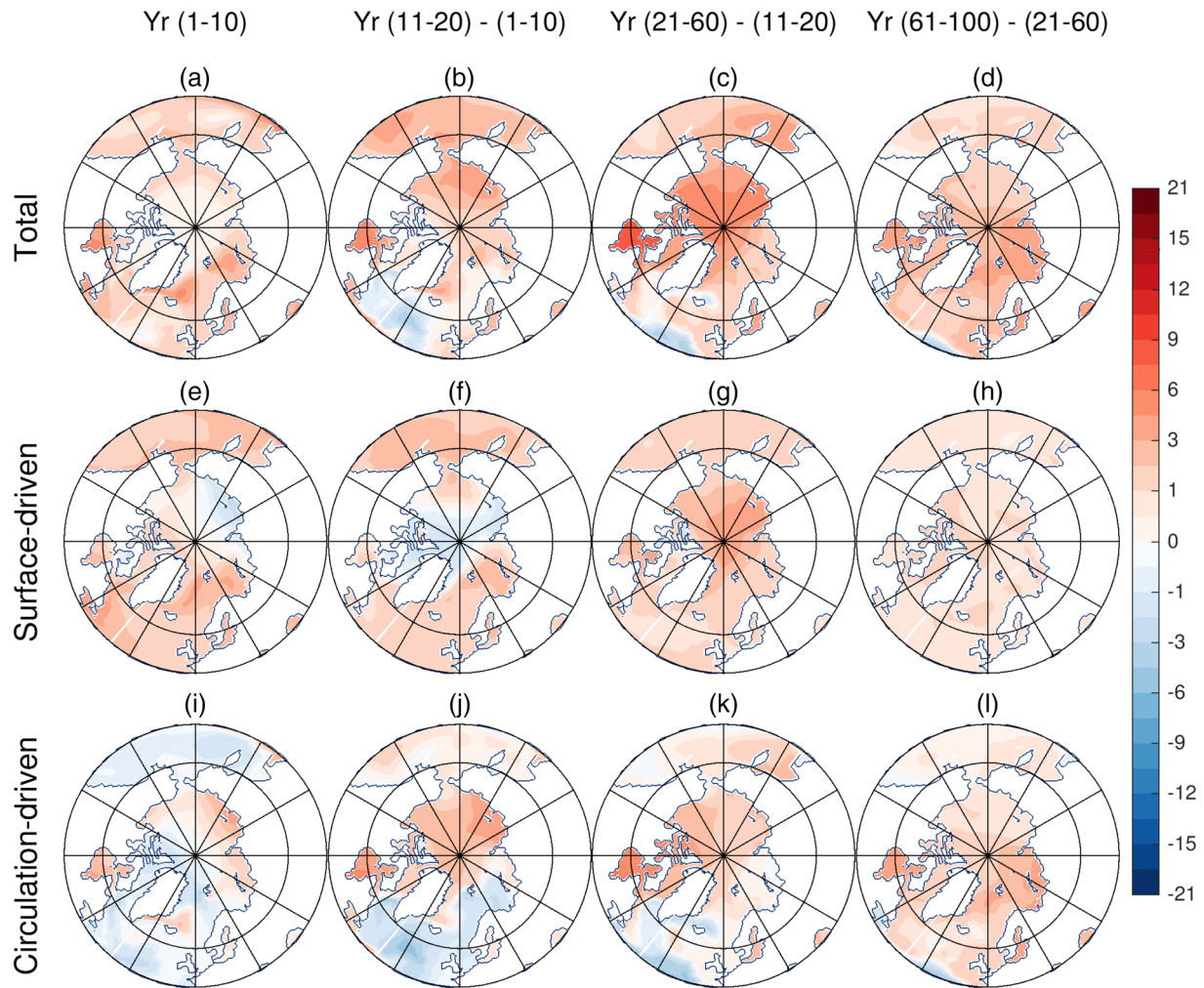
Figure 11. Winter season (DJFM) Arctic sea surface temperature anomaly (a–d) and its surface-driven component (e–h) and the circulation-driven component (i–l) for Years 1–10 (a, e, i), 11–20 (b, f, j), 20–60 (c, g, k), and 60–100 (d, h, l) in the partially coupled experiment. Units = °C.

After 20 years, the circulation-driven decrease of frazil heat stops and instead starts to increase in the fully coupled experiment, while in the partially coupled experiment, this decrease continues and causes the total loss of frazil heat around 40 years (Figure 8e red and blue lines; also compare Figures 9 and 10 [panels k and l]). This reversal of the circulation-driven decrease of frazil heat in the fully coupled experiment is also mirrored by its surface-driven component; the surface-driven increase of frazil heat also stops and starts to decline after 20 years in the fully coupled experiment (Figures 8c and 8e red lines; also compare Figures 10g, 10h and 10k, 10l). The recovery of the circulation-driven component and the compensating decline of the surface-driven component is what stops the decline of frazil heat and stabilizes Arctic sea ice bottom growth rates and area/volume in the fully coupled experiment after 20 years (compare Figures 1a, 1b, 8a, 8c, 8e red lines; 10g, 10h, 10k, and 10l). That the anomalous frazil heat components explain the different rates of Arctic sea ice volume loss in this bottom-growth-driven period in the fully and partially coupled experiments, further indicates that the anomalous winter growth rates and Arctic sea ice volume loss during this period are indeed controlled by ocean processes rather than atmosphere-ice heat fluxes.

On the other hand, in the Antarctic, the circulation-driven decrease of frazil and ocean-ice heat fluxes are very similar in both fully and partially coupled experiments, unlike those of the Arctic (Figure S9). However, as in the Arctic, the impact of the circulation-driven components is dominant, and they cause the overall decrease in frazil heat and ocean-ice heat fluxes in the Antarctic. The similar rates of the
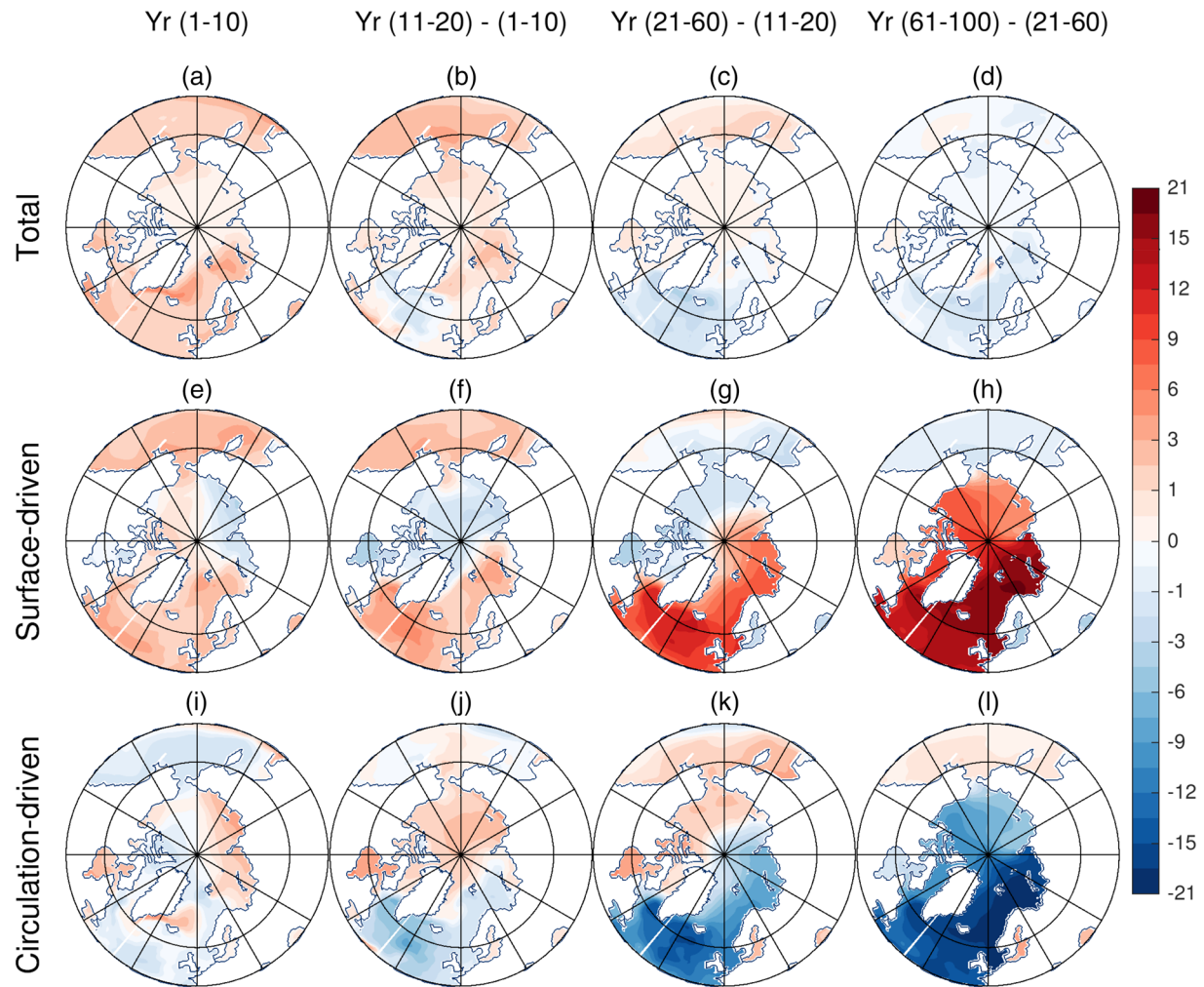
Figure 12. Same as Figure 11 but for the fully coupled experiment.

circulation-driven frazil/ocean-ice heat decrease in the Antarctic thus explain the similar rates of its sea ice volume decrease in both experiments. This similarity is consistent with the ocean circulation response over the Southern Ocean; as we will later see in section 3.4, the circulation changes in the North Atlantic are very different but very similar in the Southern Ocean in both experiments. The hemispheric differences in the ocean circulation response in both experiments thus validate that the frazil heat and ocean-ice heat flux decomposition here and also suggest that the impact of the ocean circulation changes on the air-sea interaction is not significant in the Southern ocean or that the Antarctic sea ice response is largely atmosphere driven.

3.3.2. Ocean Temperature Impact on Frazil Heat Fluxes

The anomalous frazil heat components described above are caused by the surface- and circulation-driven anomalous ocean temperature in winter shown in Figures 11 and 12 (recall Equation 4). These anomalous ocean temperature components thus provide further insight into the ocean processes driving the frazil heat component changes and validate the decomposition.

In the first 20-year period, similar rates of the circulation-driven decrease of frazil heat in the partially and fully coupled experiments are explained by similar patterns of warm circulation-driven ocean temperature anomalies that appear in winter in the Arctic in both experiments (compare Figures 9 and 10 and Figures 11 and 12 [panels i and j]). After 20 years, these warm circulation-driven winter temperature anomalies persist in the partially coupled experiment (compare Figures 9 and 11 [panels k and l]) and thereby cause the complete loss of frazil heat in this experiment. While in the fully coupled
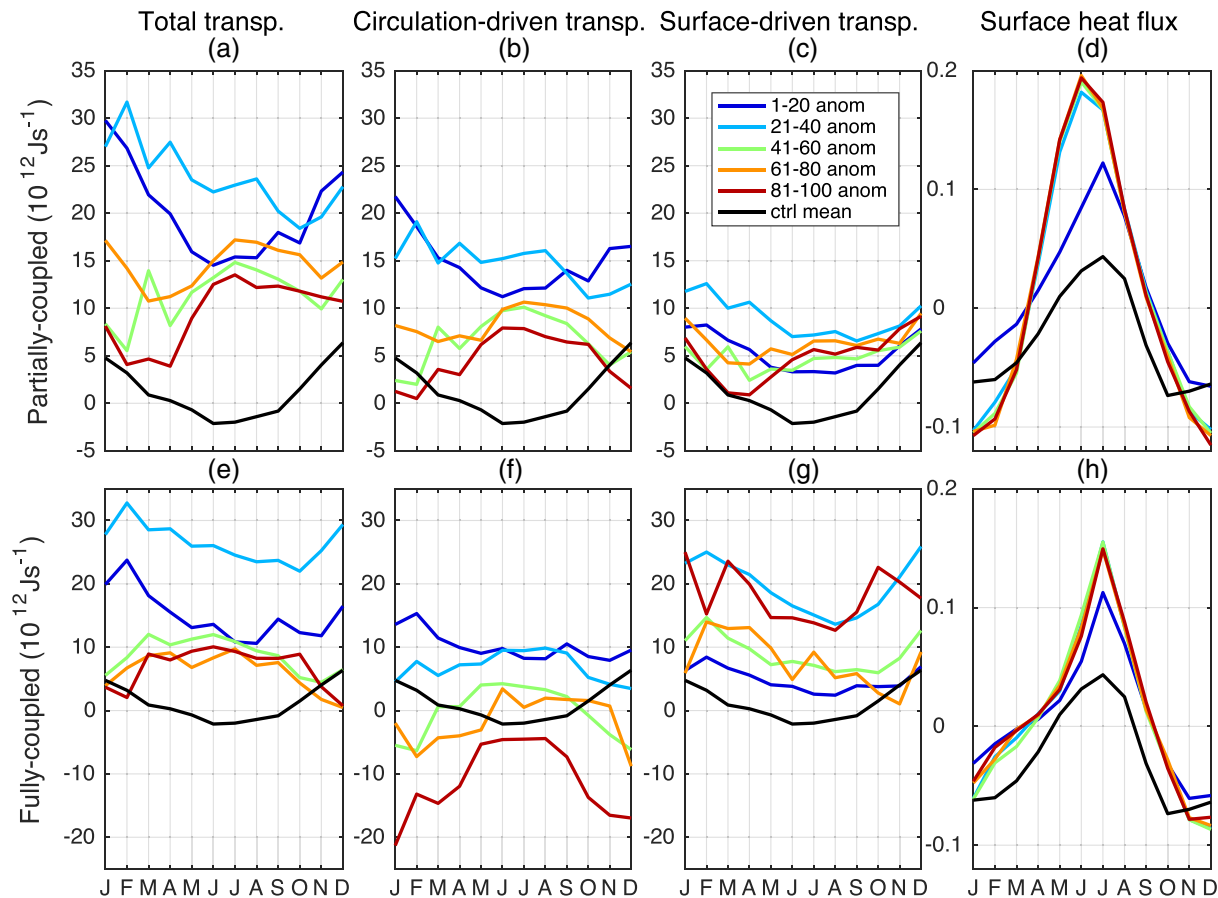
Figure 13. The Arctic Ocean heat budget decomposed into the anomalous total heat transport and its circulation- and surface-driven components and the surface heat flux. The upper row (a–d) shows terms in the partially coupled experiment. The lower row shows results for the fully coupled experiment (e–h). The control monthly (100 years) climatology is shown in each panel in black. Colored lines show the evolution of anomalies in variables over successive 20-year intervals. Heat transport is computed at the Nordic sea boundaries at 66°N, and surface heat fluxes are area-weighted poleward of 66°N.

experiment, the initial warm circulation-driven ocean temperature anomalies are replaced after 20 years by cool temperature anomalies that appear to be imported from the subpolar Atlantic. These cool circulation-driven anomalies fill the entire Arctic by the end of the 100-year experiment in the fully coupled experiment (Figures 12k and 12l). This import of cool circulation-driven temperature anomalies explains the circulation-driven increase of frazil heat in winter after 20 years in the fully coupled experiment (Figure 8e red line and Figures 10k and 10l).

In contrast, cool surface-driven ocean temperature anomalies appear in the Arctic in the first 20 years (Figures 11 and 12 [panels e and f]), which cause the initial surface-driven increase in frazil heat in both experiments (Figures 8c and Figures 9 and 10 [panels e and f]). After the initial 20-year period, these cool winter surface-driven anomalies are also replaced by warm surface-driven temperature anomalies in both experiments (Figures 11 and 12 [panels g and h]). However, in the partially coupled experiment, the warm surface-driven anomalies quickly fill the Arctic in place of the cool ones (Figures 11g and 11h), which explains the rapid decline of the surface-driven increase in frazil heat in this experiment (Figure 8c blue line and Figures 9g and 9h). In the fully coupled experiment, warm surface-driven temperature anomalies that appear to be compensating the cool circulation-driven temperature anomalies are also imported from the subpolar Atlantic, and they gradually replace the initial cool temperature anomalies as they are transported into the Arctic (compare Figures 12g, 12h, 12k, and 12l). These remote warm surface-driven temperature anomalies explain the gradual surface-driven decrease in frazil heat in the fully coupled experiment after 20 years (compare Figure 8c red line and Figures 10g and 10h). The time-evolving patterns of the

anomalous temperature components in the fully and partially coupled experiments thus suggest that remote ocean temperature changes in the subpolar Atlantic have significant consequences on Arctic sea ice changes.

3.4. Local and Remote Influences on Arctic Frazil/Ocean-Ice Heat Fluxes

In order to understand the relative impacts of the local and remote ocean processes on Arctic frazil heat or frazil growth decrease, we examine the anomalous surface heat fluxes and anomalous heat transport into the Arctic (Figure 13). According to Equations 9 and 10, the surface- and circulation-driven anomalous ocean temperature components include impacts from local surface heat flux and ocean circulation changes in the Arctic (i.e., Q' and $v' \cdot \nabla \overline{T}_O$ terms), as well as impacts from remote surface heat flux and ocean circulation changes through ocean heat convergence terms (i.e., $v \cdot \nabla T'_{OQ}$ and $v \cdot \nabla T'_{OO}$). We focus on the surface heat flux anomalies poleward of the 66°N and diagnose the net anomalous ocean heat transport as the difference between the perturbed and control experiments' meridional ocean heat transport into the Arctic through the Nordic Sea boundaries at 66°N (where most of the heat transport into the Arctic occurs; i.e., $v \cdot \nabla T_O - \overline{v} \cdot \nabla \overline{T}_O = v' \cdot \nabla \overline{T}_O + v \cdot \nabla T'_{OQ} + v \cdot \nabla T'_{OO}$). The surface-driven anomalous ocean heat transport component is computed using the meridional transport of the tracer P_1 into the Arctic (i.e., $v \cdot \nabla P_1$; recall $P_1 = T'_{OQ}$), while the circulation-driven component is the difference between the meridional transport of tracer P_2 and the baseline meridional heat transport into the Arctic (i.e., $v \cdot \nabla P_2 - \overline{v} \cdot \nabla \overline{T}_O = v' \cdot \nabla \overline{T}_O + v \cdot \nabla T'_{OO}$; recall $P_2 = T'_{OO} + \overline{T}_O$; see section 2.2.3).

In the first 20-year period, the circulation-driven component contributes the larger proportion of the anomalous heat transport into the Arctic in both experiments, especially in winter (compare Figures 13b and 13c with Figures 13f and 13g, deep blue lines). This large circulation-driven increase in the ocean heat transport into the Arctic in winter explains the initial warm circulation-driven winter temperature anomalies and the large circulation-driven decrease of the ocean-ice heat fluxes that occur in the first 20-year period in both experiments (Figures 9–12, panels i and j). By definition, circulation-driven heat transport anomalies include the impacts of both local and remote ocean circulation changes ($v' \cdot \nabla \overline{T}_O$ and $v \cdot \nabla T'_{OO}$ in Equation 10). However, since they have an immediate impact on Arctic temperatures, this initial circulation-driven anomalous heat transport into the Arctic likely results from the redistribution of the baseline Arctic temperature gradient by local Arctic ocean circulation changes (i.e., $v' \cdot \nabla \overline{T}_O$ term) rather than from the import of remote circulation-driven ocean temperature anomalies ($v \cdot \nabla T'_{OO}$ term). Heat transport into the Arctic occurs largely through the Atlantic inflow into the Arctic, which occurs below the mixed layer in the cold halocline layer and so should not immediately have an impact on mixed-layer temperature (Aagaard et al., 1981; Steele et al., 1995).

On the other hand, surface-driven ocean temperature anomalies can be produced by both local anomalous surface heat fluxes and transport of remote surface-driven temperature anomalies into the Arctic (i.e., Q' and $v \cdot \nabla T'_{OQ}$ in Equation 9). Though weaker than the circulation-driven anomalous heat transport, the Arctic also gains heat through the import of remote surface-driven ocean temperature anomalies in both experiments, especially in winter (Figures 13c and 13g), while it loses heat through an anomalous increase in surface heat loss in winter and gains anomalous surface heat in summer (Figures 13d and 13h). These anomalous winter surface heat loss and summer surface heat gain are caused by the new open waters that result from sea ice loss in the Arctic (not shown). This additional surface heat exchange in new open waters explains why the partially coupled experiment has greater anomalous surface heat fluxes than the fully coupled experiment after 20 years since the Arctic has a smaller sea ice extent after 10 years in this experiment (compare Figures 13d and 13h).

The initial surface-driven cooling of Arctic winter ocean temperatures and increase of frazil heat in the first 20-year period (recall Figures 11 and 12 and Figures 9 and 10 [panels e and f]) are thus explained by the local anomalous Arctic surface heat loss in winter, rather than the import of remote surface-driven ocean temperature anomalies from the subpolar Atlantic ($v \cdot \nabla T'_{OQ}$). Though the energy input by the local anomalous surface heat fluxes is much weaker than that by anomalous surface-driven heat transport (compare the magnitudes in Figures 13c and 13g and Figures 13d and 13h), the surface-driven anomalous heat transports into the Arctic do not have an immediate impact on Arctic temperature changes. Similar to the remote circulation-driven anomalies, the transport of remote surface-driven anomalies also has a
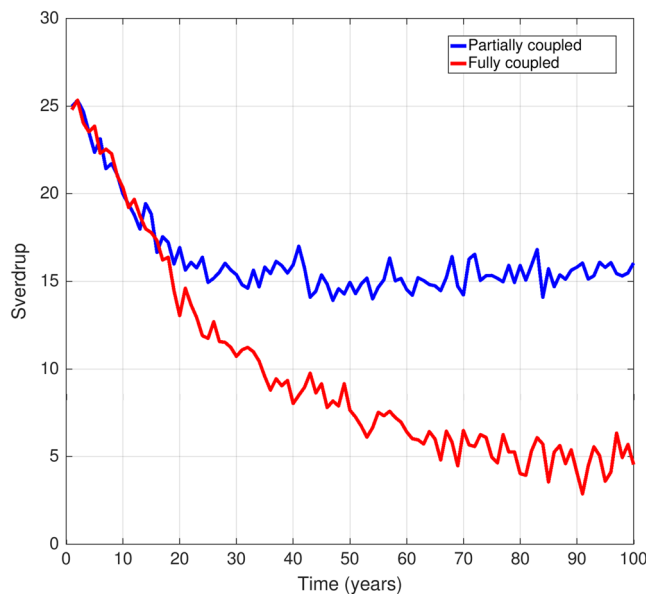
Figure 14. Time series of the Atlantic meridional overturning circulation (AMOC) index in the partially coupled (blue) and fully coupled (red) experiments. The AMOC index is defined at the location of maximum volume at latitudes north of 26°N and depth greater than 500 m.

delayed impact on Arctic temperatures because they are also transported through the Atlantic inflow below the Arctic mixed layer.

After the initial 20-year period, the circulation-driven increase of the anomalous heat transport attenuates in both experiments, particularly in winter (Figures 13b and 13f, light blue to red lines). However, in the fully coupled experiment, the attenuation of the circulation-driven anomalous heat transport occurs at a much faster rate and eventually causes the Arctic to lose heat in winter (Figure 13f, light blue to red lines). These differing attenuation rates of the circulation-driven heat transports after 20 years explain the slower circulation-driven decrease of frazil heat in the partially coupled experiment and its recovery in the fully coupled experiment after the initial 20-year period (recall Figure 8e). As the circulation-driven ocean temperature anomaly pattern suggests, the reversal of the anomalous heat transport into the Arctic in the fully coupled experiment after 20 years is caused by the import of remote cool circulation-driven ocean temperature anomalies from the subpolar Atlantic through the Atlantic inflow (i.e., $v \cdot \nabla T'_{OO}$ term; compare Figures 12k and 12l), which can now reach the Arctic mixed layer possibly through a gradual retreat of the cold halocline layer (Steele & Boyd, 1998).

Similarly, the import of remote surface-driven ocean temperature anomalies also reaches the Arctic mixed layer and causes the emergence of warm surface-driven temperature anomalies in the Arctic after 20 years in both experiments (Figures 11 and 12 [panels g and h]). This surface-driven warming of the Arctic occurs despite the sustained increase in winter surface heat loss during this period (Figures 13d and 13h). As a result of warm surface-driven temperature anomalies that act to compensate the large circulation-driven cooling in the subpolar Atlantic in the fully coupled experiment, the surface-driven ocean heat transport after 20 years is also greater in the fully coupled experiment (compare Figures 13c and 13g and Figures 12g, 12h, 12k, and 12l). Compensation between the circulation- and surface-driven temperature components in the fully coupled experiment is consistent with two-way air-sea interaction in this experiment: Circulation-driven ocean temperature anomalies are coupled to the atmosphere in the fully coupled experiment, thereby allowing anomalous heat fluxes to compensate for and oppose these circulation-driven surface temperature anomalies. In the partially coupled experiment, the coupling with the circulation-driven component is suppressed such that there is no compensation between its surface- and circulation-driven temperature anomalies.

Our analysis thus suggests that ocean circulation changes play a dominant role in ocean-driven Arctic sea ice changes both in the initial decrease and subsequent stabilization of the sea ice in the fully coupled experiment. Local ocean circulation changes in the Arctic cause an initial increase in ocean heat transport into the Arctic and a resulting decrease of frazil ice growth in winter, while remote ocean circulation changes in the subpolar Atlantic prevent the total decline of sea ice growth in winter through the transport of the circulation-driven subpolar Atlantic temperature anomalies into the Arctic. Local anomalous surface heat loss in the Arctic also increases in winter due to new open waters that appear from the loss of sea ice cover but only play a role in sea ice winter growth recovery in the short term. The impact of this increased surface heat loss is weakened by the export of remote surface-driven temperature anomalies into the Arctic after 20 years. Consistent with the ice-albedo feedback mechanism, anomalous surface heat gain due to new open waters in summer also increases ocean-ice heat fluxes (Figure 8d), but their impact is also small compared to the circulation-driven sea volume loss, which causes an overall decrease in melt and ocean-ice heat fluxes (Figures 8d and 8f). The impact of ocean circulation changes on the local air-sea interaction and anomalous surface heat fluxes in the Arctic is also weak. The differences between anomalous surface heat fluxes in the Arctic in the partially and fully coupled experiments are better explained by the differences in the sea ice cover.

The cooling of the subpolar Atlantic in global warming experiments and observations has been associated with the weakening of the Atlantic meridional overturning circulation (AMOC) (Garuba et al., 2018;

Gervais et al., 2018; Maroon et al., 2018; Winton et al., 2013). Consistent with this mechanism, the AMOC weakens a lot more in the fully coupled experiment than in the partially coupled one, particularly after 20 years (Figure 14), therefore explaining the greater subpolar Atlantic cooling and reversal of the ocean heat transport into the Arctic after 20 years in this experiment. That the AMOC weakens more in the fully coupled experiment than the partially coupled one suggests that the coupled two-way atmosphere-ocean interaction enhances AMOC weakening response to CO_2 increase. In contrast, the impact of the coupled atmosphere-ocean interaction is weak in the Southern Hemisphere, and the ocean circulation response is very similar in both experiments. The ocean circulation response in the Southern Ocean is primarily caused by the poleward shift of the Southern Ocean winds (See Figure 11 and further discussion of surface flux response in GR20). The similarity between the ocean circulation response in the Southern Ocean also explains the similarities in circulation-driven frazil/ocean-ice heat fluxes and Antarctic sea ice loss in both experiments (Figures 1c, 1d, and S9) and further validates our decomposition.

The greater weakening of the AMOC in the fully coupled experiment is likely caused by the compensation of the circulation-driven cooling of the subpolar Atlantic by anomalous surface heat fluxes. Circulation-driven cooling of the subpolar Atlantic provides a negative feedback (or temperature advective feedback) that stabilizes the AMOC and prevents further weakening. The compensation of the circulation-driven cooling in the subpolar Atlantic thereby suppresses the stabilizing impact of the temperature advective feedback, while it enhances the destabilizing impact of the circulation-driven freshening of the subpolar Atlantic on the AMOC (salinity advective feedback) and thereby causes further weakening of the AMOC. The details of the coupled AMOC weakening response is beyond the scope of this paper and will be explored in future work. Nevertheless, the results here suggest that this coupled feedback impact on AMOC weakening results from the atmosphere-ocean interaction rather than ocean-ice interactions. The partially coupled experiment completely loses its sea ice and yet has a smaller weakening of the AMOC than the fully coupled experiment that has partial loss of its sea ice.

4. Summary and Discussion

We use a novel decomposition of the anomalous ocean heat energy used for frazil ice growth and sea ice melt (frazil/ocean-ice heat fluxes) and a sea ice volume budget analysis to disentangle the atmosphere-ocean-ice interactions driving Arctic sea ice response to CO_2 quadrupling. The sea ice volume budget analysis is used to isolate atmosphere- and ocean-driven Arctic sea ice volume changes caused by anomalous atmosphere-ice heat fluxes and frazil/ocean-ice heat fluxes, respectively. The anomalous frazil heat and ocean-ice heat fluxes are further decomposed into components that are caused by anomalous surface heat fluxes (surface-driven) and ocean circulation changes (circulation-driven) in the Arctic using temperature-like tracers in partially and fully coupled global climate model experiments. Arctic sea ice volume budget and frazil/ocean-ice heat flux components are compared between the partially and fully coupled experiments to isolate how the coupling between the atmosphere and ocean also modifies the atmosphere- and ocean-driven sea changes.

The Arctic sea ice volume budget analysis here suggests that the atmosphere drives most Arctic sea ice loss in the short term (within a decade) by increasing Arctic sea ice top face melt, while the ocean plays a greater role in the long term (beyond 10 years) by decreasing sea ice growth in winter (Figure 3). Though atmosphere-ice heat fluxes drive most of sea ice growth in winter through conduction or basal growth, an overall decrease in sea ice growth in winter occurs due to the decrease in net sea ice area available for basal growth, as a result of the decrease in the ocean-driven frazil ice growth; basal ice growth itself increases where sea ice concentration has not declined. The surface- and circulation-driven frazil heat components further show that this ocean-driven decrease occurs largely through its circulation changes, which cause an increase in ocean heat convergence into the Arctic, particularly in the winter. Anomalous surface heat loss (gain) due to the shrinking sea ice area instead increases winter (summer) growth (melt). However, these play a smaller role in the short term because the impact of the circulation-driven heat convergence in winter is greater (Figure 5).

Comparing the frazil heat components in the partially and fully coupled experiments further shows that the ocean-circulation-driven decrease in winter ice growth is eventually stabilized by the atmosphere-ocean coupling in the subpolar Atlantic in the fully coupled experiment. Air-sea interactions in the subpolar North

Atlantic serve as a negative feedback on sea ice loss by accelerating the weakening of the AMOC and its resulting cooling of the subpolar Atlantic; these cool circulation-driven temperature anomalies are later exported into the Arctic, thereby causing the attenuation of the initial increase in ocean heat transport into the Arctic in winter and the decline in frazil heat associated with it. Without this export of the circulation-driven cooling of the subpolar amplified by the two-way air-sea interaction impact on ocean circulation changes, the initial anomalous increase in heat transport into the Arctic in winter causes the total loss of Arctic sea ice in the partially coupled experiment. Interestingly, this coupled feedback on the ocean circulation change does not occur in the Southern Ocean, and as a result, it also has little impact on Antarctic sea ice loss, suggesting these are not spurious results from the partially coupled experiment.

The results here are consistent with earlier studies of sea ice volume budget analysis. The bottom-growth-driven Arctic sea ice loss in the long term is also found in the multimodel study of Holland et al. (2010). Our attribution of the decrease in sea ice bottom growth to decreasing frazil ice formation rather than to conductive growth by atmosphere-ice heat fluxes is consistent with what is found in the Hadgem model study of Keen and Blockley (2018) and West et al. (2013). The surface-driven increase in winter sea ice growth seen here is also similar to the sea ice recovery mechanism shown in the study of Tietsche et al. (2011), where total sea ice loss caused by imposing large summer melting recovers as a result of increased growth in winter due to the anomalous surface heat loss. However, here the impact of this surface-driven increase in growth is short-lived and weaker than the circulation-driven decrease in growth. Similarly, the results here suggest that the ice-albedo feedback mechanism, which has been proposed for accelerating sea ice loss through the anomalous surface heat gain in summer (Curry et al., 1995; Perovich et al., 2007), might be weak in the presence of large ocean heat transports in winter, as winter bottom growth decrease reduces the overall sea ice volume available for melt. We also note that the impact of heat transport into the Arctic also depends on the integrity of the cold halocline, which prevents Atlantic heat intrusion into the Arctic to be entrained into the mixed layer (Steele et al., 1995, 2008).

An important result of this study is the eventual stabilization of Arctic sea ice loss after an initial phase of increase in ocean heat transport into the Arctic. The initial phase of the increase in winter heat transport into the Arctic caused by the weakening of the AMOC has been noted in other studies and in observations (Årthun et al., 2019; Auclair & Tremblay, 2018; Oldenburg et al., 2018; Polyakov et al., 2017; Singh et al., 2017). The reversal of this circulation-driven increase of winter heat transport shown here implies that the continual weakening of the AMOC and resulting cooling of the subpolar Atlantic may prevent the complete loss of Arctic sea ice. This result also implies that better representation of the coupled ocean circulation response in the subpolar Atlantic is very important for accurate model representation of Arctic sea ice changes, especially over longer time scales. Indeed, a slowdown of Arctic sea ice loss due to continued AMOC weakening has been noted in a recent predictability study of historical simulations (Yeager et al., 2015). Petty et al. (2018) also report a negative correlation between ocean temperatures and sea ice growth initially, which changes to a positive correlation with time in historical simulations, in agreement with the results here.

However, our result of the coupled air-sea interaction feedback on the AMOC weakening and its impact in stabilizing Arctic sea ice loss might appear to be at odds with the previous attribution of the weakening of the AMOC to anomalous freshwater fluxes from Arctic sea ice loss (Liu et al., 2019; Svellec & Fedorov, 2016; Svellec et al., 2017). Here, the relatively smaller weakening of the AMOC despite the total loss of Arctic sea ice in the partially coupled experiment suggests that the impact of freshwater flux changes on the AMOC weakening is small. Instead, the feedback on AMOC weakening, which permits Arctic sea ice stabilization, occurs through air-sea coupling in the subpolar Atlantic. While the negative feedback on sea ice loss due to the AMOC weakening is also observed in the experiment with large AMOC weakening in the Liu et al. (2019) study, its impact is weaker. The different conclusions in both studies might be due to different forcing mechanisms used for driving AMOC weakening in both studies. Arctic sea ice changes were imposed by changing sea ice radiative properties in the study of Liu et al. (2019), so the freshwater flux change is the dominant surface flux perturbation that the AMOC responds to, while in this study, CO_2 quadrupling largely causes surface heat fluxes changes. Anomalous surface heat fluxes have been shown to have a greater impact on the AMOC response than freshwater fluxes in global warming experiments (Garuba & Klinger, 2018; Gregory et al., 2016). This may explain why the air-sea interaction feedback on AMOC response is

dominant in our experiment. These differences therefore suggest relative strengths of the atmosphere-ocean and ocean-ice feedbacks of the Arctic sea ice might be dependent on the forcing mechanisms.

It is important to note some important caveats of the present study. First, we have ignored the impact of sea ice loss by advection in the analysis and have only focused on the thermodynamic changes driving sea ice loss; the former may prove to be quite important regionally in the Arctic, but sea ice loss by advection does not contribute to the global budget considered here. Furthermore, the results presented here are based on one model and an idealized forcing (abruptly quadrupled CO_2) and may therefore be an imperfect analog to present-day changes in sea ice. Despite these issues, our work provides a greater understanding of the evolving roles of the atmosphere and ocean in the sea ice response to global warming, which might be obscured by atmosphere-ocean-ice interactions in standard forced experiments driven by historical or future increases in CO_2 concentrations, or obscured by interannual variability in observed Arctic sea ice changes.

Appendix A: Tracer Initializations and Surface Forcings

Two tracers are introduced in each experiment to isolate the surface- and circulation-driven anomalous ocean temperature components (Equations 9 and 10). The first tracer denoted as P_1 is designed to isolate the surface-driven anomalous ocean temperature T'_{OQ}. According to Equation 9, T'_{OQ} is forced by the anomalous surface heat fluxes (Q') in the perturbed experiment, and at the initial time when CO_2 perturbation is turned on in the experiments, Q' would be zero, and so will T'_{OQ}. Similarly, tracer P_1 is set to equal zero at initialization and forced with Q' from the perturbed experiment. To force P_1, Q' is computed online in the perturbed experiment as the difference between the surface heat fluxes in the experiment and the baseline surface heat flux from the control experiment (i.e., $Q' = Q - \overline{Q}$). Note that $\overline{Q}$ is supplied as input as the monthly averaged model output of the surface heat fluxes ("SHF"). However, in CESM, SHF includes the melt ocean-ice heat flux ("MELTH_F"), so $\overline{Q}$ is computed as $\text{SHF} - \text{MELTH\_F}$. The tracer tendency equation for P_1 solved by the model is thus equal to Equation 9, and $P_1 = T'_{OQ}$.

In order to isolate the circulation-driven anomalous component T'_{OO}, the second tracer (P_2) is designed to emulate the baseline ocean temperature ($\overline{T}_O$), described by Equation 7. P_2 is thus set equal to $\overline{T}_O$ at the initial time, and like $\overline{T}_O$, P_2 is also forced with $\overline{Q}$ (from the control experiment). The tendency equation for P_2 solved by the model is thus similar to the baseline tendency Equation 7, except that P_2 is subject to a different ocean transport strength because P_2 evolves in a perturbed experiment (i.e., $v \cdot \nabla P_2 \neq \overline{v} \cdot \nabla \overline{T}_O$). As a result, tracer P_2 evolves differently from the baseline (control) temperature field over time. It can be shown that the difference between P_2 and $\overline{T}_O$ is equal to the circulation-driven ocean temperature anomaly (i.e., $P_2 = \overline{T}_O + T'_{OO}$; see Appendix B in GR20 for derivation). The sum of the two tracers is thus equal to the actual ocean temperature (i.e., $P_1 + P_2 = T'_{OQ} + T'_{OO} + \overline{T}_O = T_O$; see Figure B1 of GR20 for a comparison of the actual ocean temperature and the sum of the tracers).

Data Availability Statement

The model output for the control simulation data is available on the HPSS at NCAR: /CCSM/csm/b.e11. B1850C5CN.f09_g16.005; perturbed simulation data can be downloaded at https://doi.org/10.5281/ zenodo.3593507 and https://doi.org/10.5281/zenodo.3666000.

References

Aagaard, K., Coachman, L. K., & Carmack, E. (1981). On the halocline of the Arctic Ocean. *Deep Sea Research Part A. Oceanographic Research Papers*, *28*(6), 529–545.

Årthun, M., Eldevik, T., & Smedsrud, L. H. (2019). The role of Atlantic heat transport in future Arctic winter sea ice loss. *Journal of Climate*, *32*(11), 3327–3341.

Auclair, G., & Tremblay, L. B. (2018). The role of ocean heat transport in rapid sea ice declines in the Community Earth System Model large ensemble. *Journal of Geophysical Research: Oceans*, *123*, 8941–8957. https://doi.org/10.1029/2018JC014525

Banks, H. T., & Gregory, J. M. (2006). Mechanisms of ocean heat uptake in a coupled climate model and the implications for tracer based predictions of ocean heat uptake. *Geophysical Research Letters*, *33*, L07608. https://doi.org/10.1029/2005GL025352

Bitz, C. M., Gent, P. R., Woodgate, R. A., Holland, M. M., & Lindsay, R. (2006). The influence of sea ice on ocean heat uptake in response to increasing CO_2. *Journal of Climate*, *19*(11), 2437–2450.

Bitz, C. M., Holland, M. M., Hunke, E. C., & Moritz, R. E. (2005). Maintenance of the sea-ice edge. *Journal of Climate*, *18*(15), 2903–2921. https://doi.org/10.1175/JCLI3428.1

Bitz, C. M., & Roe, G. H. (2004). A mechanism for the high rate of sea ice thinning in the Arctic Ocean. *Journal of Climate*, *17*(18), 3623–3632. https://doi.org/10.1175/1520-0442(2004)017<3623:AMFTHR>2.0.CO;2

Bitz, C. M., Shell, K. M., Gent, P. R., Bailey, D. A., Danabasoglu, G., Armour, K. C., et al. (2012). Climate sensitivity of the Community Climate System Model, version 4. *Journal of Climate*, *25*(9), 3053–3070.

Bracegirdle, T. J., Hyder, P., & Holmes, C. R. (2018). CMIP5 diversity in southern westerly jet projections related to historical sea ice area: Strong link to strengthening and weak link to shift. *Journal of Climate*, *31*(1), 195–211.

Burgard, C., & Notz, D. (2017). Drivers of Arctic Ocean warming in CMIP5 models. *Geophysical Research Letters*, *44*, 4263–4271. https://doi.org/10.1002/2016GL072342

Curry, J. A., Schramm, J. L., & Ebert, E. E. (1995). Sea ice-albedo climate feedback mechanism. *Journal of Climate*, *8*(2), 240–247.

Danabasoglu, G., Bates, S. C., Briegleb, B. P., Jayne, S. R., Jochum, M., Large, W. G., et al. (2012). The CCSM4 ocean component. *Journal of Climate*, *25*(5), 1361–1389.

Ding, Y., Carton, J. A., Chepurin, G. A., Steele, M., & Hakkinen, S. (2016). Seasonal heat and freshwater cycles in the Arctic Ocean in CMIP5 coupled models. *Journal of Geophysical Research: Oceans*, *121*, 2043–2057. https://doi.org/10.1002/2015JC011124

Dmitrenko, I. A., Polyakov, I. V., Kirillov, S. A., Timokhov, L. A., Frolov, I. E., Sokolov, V. T., et al. (2008). Toward a warmer Arctic Ocean: Spreading of the early 21st century Atlantic water warm anomaly along the Eurasian basin margins. *Journal of Geophysical Research*, *113*, C05023. https://doi.org/10.1029/2007JC004158

Francis, J. A., & Hunter, E. (2006). New insight into the disappearing Arctic sea ice. *Eos, Transactions American Geophysical Union*, *87*(46), 509–511. https://doi.org/10.1029/2006EO460001

Gabison, R. (1987). A thermodynamic model of the formation, growth, and decay of first-year sea ice. *Journal of Glaciology*, *33*(113), 105–119.

Garuba, O. A., & Klinger, B. A. (2018). The role of individual surface flux components in the passive and active ocean heat uptake. *Journal of Climate*, *31*(15), 6157–6173. https://doi.org/10.1175/JCLI-D-17-0452.1

Garuba, O. A., Lu, J., Liu, F., & Singh, H. A. (2018). The active role of the ocean in the temporal evolution of climate sensitivity. *Geophysical Research Letters*, *45*, 306–315. https://doi.org/10.1002/2017GL075633

Garuba, O. A., & Rasch, P. J. (2020). A partial coupling method to isolate the roles of the atmosphere and ocean in coupled climate simulations. *Journal of Advances in Modeling Earth Systems*, *12*, e2019MS002016. https://doi.org/10.1029/2019MS002016

Gervais, M., Shaman, J., & Kushnir, Y. (2018). Mechanisms governing the development of the North Atlantic warming hole in the CESM-LE future climate simulations. *Journal of Climate*, *31*(15), 5927–5946. https://doi.org/10.1175/JCLI-D-17-0635.1

Goosse, H., Kay, J. E., Armour, K. C., Bodas-Salcedo, A., Chepfer, H., Docquier, D., et al. (2018). Quantifying climate feedbacks in polar regions. *Nature Communications*, *9*(1), 1919.

Gregory, J. M., Bouttes, N., Griffies, S. M., Haak, H., Hurlin, W. J., Jungclaus, J., et al. (2016). The Flux-Anomaly-Forced Model Intercomparison Project (FAFMIP) contribution to CMIP6: investigation of sea-level and ocean climate change in response to CO_2 forcing. *Geoscientific Model Development*, *9*(11), 3993–4017. https://doi.org/10.5194/gmd-9-3993-2016

Holland, M. M., Bitz, C. M., & Tremblay, B. (2006). Future abrupt reductions in the summer Arctic sea ice. *Geophysical Research Letters*, *33*, L23503. https://doi.org/10.1029/2006GL028024

Holland, M. M., Serreze, M. C., & Stroeve, J. (2010). The sea ice mass budget of the Arctic and its future change as simulated by coupled climate models. *Climate Dynamics*, *34*(2), 185–200. https://doi.org/10.1007/s00382-008-0493-4

Hunke, E. C., Lipscomb, W. H., Turner, A. K., Jeffery, N., & Elliott, S. (2010). CICE: The Los Alamos sea ice model documentation and software user's manual version 4.1 la-cc-06-012. T-3 Fluid Dynamics Group, Los Alamos National Laboratory.

Hwang, Y.-T., Frierson, D. M. W., & Kay, J. E. (2011). Coupling between Arctic feedbacks and changes in poleward energy transport. *Geophysical Research Letters*, *38*, L17704. https://doi.org/10.1029/2011GL048546

Kay, J. E., Holland, M. M., Bitz, C. M., Blanchard-Wrigglesworth, E., Gettelman, A., Conley, A., & Bailey, D. (2012). The influence of local feedbacks and northward heat transport on the equilibrium Arctic climate response to increased greenhouse gas forcing. *Journal of Climate*, *25*(16), 5433–5450.

Kay, J. E., L'Ecuyer, T., Gettelman, A., Stephens, G., & O'Dell, C. (2008). The contribution of cloud and radiation anomalies to the 2007 Arctic sea ice extent minimum. *Geophysical Research Letters*, *35*, L08503. https://doi.org/10.1029/2008GL033451

Keen, A., & Blockley, E. (2018). Investigating future changes in the volume budget of the Arctic sea ice in a coupled climate model. *Cryosphere*, *12*(9), 2855–2868.

Liu, W., Fedorov, A., & Sévellec, F. (2019). The mechanisms of the Atlantic meridional overturning circulation slowdown induced by Arctic sea ice decline. *Journal of Climate*, *32*(4), 977–996.

Maroon, E. A., Kay, J. E., & Karnauskas, K. B. (2018). Influence of the Atlantic meridional overturning circulation on the Northern Hemisphere surface temperature response to radiative forcing. *Journal of Climate*, *31*(22), 9207–9224.

Martinson, D. G., & Iannuzzi, R. A. (1998). Antarctic ocean-ice interaction: Implications from ocean bulk property distributions in the Weddell gyre. *Antarctic Sea Ice: Physical Processes, Interactions and Variability*, *74*, 243–271.

Maslanik, J., Drobot, S., Fowler, C., Emery, W., & Barry, R. (2007). On the arctic climate paradox and the continuing role of atmospheric circulation in affecting sea ice conditions. *Geophysical Research Letters*, *34*, L03711. https://doi.org/10.1029/2006GL028269

Mayer, M., Haimberger, L., Pietschnig, M., & Storto, A. (2016). Facets of arctic energy accumulation based on observations and reanalyses 2000–2015. *Geophysical Research Letters*, *43*, 10,420–10,429. https://doi.org/10.1002/2016GL070557

Neale, R. B., Chen, C.-C., Gettelman, A., Lauritzen, P. H., Park, S., Williamson, D. L., et al. (2010). Description of the NCAR Community Atmosphere Model (CAM 5.0). NCAR Tech. Note NCAR/TN-486+ STR.

Nummelin, A., Li, C., & Hezel, P. J. (2017). Connecting ocean heat transport changes from the midlatitudes to the Arctic Ocean. *Geophysical Research Letters*, *44*, 1899–1908. https://doi.org/10.1002/2016GL071333

Oldenburg, D., Armour, K. C., Thompson, L., & Bitz, C. M. (2018). Distinct mechanisms of ocean heat transport into the Arctic under internal variability and climate change. *Geophysical Research Letters*, *45*, 7692–7700. https://doi.org/10.1029/2018GL078719

Oleson, K. W., Lawrence, D. M., Gordon, B., Flanner, M. G., Kluzek, E., Peter, J., et al. (2010). Technical description of version 4.0 of the Community Land Model (CLM) (*NCAR Tech note No. NCAR/TN-478+STR*).

Perovich, D. K., Light, B., Eicken, H., Jones, K. F., Runciman, K., & Nghiem, S. V. (2007). Increasing solar heating of the Arctic Ocean and adjacent seas, 1979–2005: Attribution and role in the ice-albedo feedback. *Geophysical Research Letters*, *34*, L19505. https://doi.org/10.1029/2007GL031480

Petty, A. A., Holland, M. M., Bailey, D. A., & Kurtz, N. T. (2018). Warm Arctic, increased winter sea ice growth? *Geophysical Research Letters*, *45*, 12,922–12,930. https://doi.org/10.1029/2018GL079223

Polyakov, I. V., Beszczynska, A., Carmack, E. C., Dmitrenko, I. A., Fahrbach, E., Frolov, I. E., et al. (2005). One more step toward a warmer Arctic. *Geophysical Research Letters*, *32*, L17605. https://doi.org/10.1029/2005GL023740

Polyakov, I. V., Pnyushkov, A. V., Alkire, M. B., Ashik, I. M., Baumann, T. M., Carmack, E. C., et al. (2017). Greater role for Atlantic inflows on sea-ice loss in the Eurasian basin of the Arctic Ocean. *Science*, *21*, 285–291. https://doi.org/10.1126/science.aai8204

Semtner, A. J. Jr. (1976). A model for the thermodynamic growth of sea ice in numerical investigations of climate. *Journal of Physical Oceanography*, *6*(3), 379–389.

Serreze, M. C., Holland, M. M., & Stroeve, J. (2007). Perspectives on the Arctic's shrinking sea-ice cover. *Science*, *315*(5818), 1533–1536.

Singh, H. A., Garuba, O. A., & Rasch, P. J. (2018). How asymmetries between Arctic and Antarctic climate sensitivity are modified by the ocean. *Geophysical Research Letters*, *45*, 13,031–13,040. https://doi.org/10.1029/2018GL079023

Singh, H. A., Rasch, P. J., & Rose, B. E. J. (2017). Increased ocean heat convergence into the high latitudes with CO_2 doubling enhances polar-amplified warming. *Geophysical Research Letters*, *44*, 10,583–10,591. https://doi.org/10.1002/2017GL074561

Smith, R., Jones, P., Briegleb, B., Bryan, F., Danabasoglu, G., Dennis, J., et al. (2010). The Parallel Ocean Program (POP) reference manual: Ocean component of the Community Climate System Model (CCSM) and Community Earth System Model (CESM). LAUR-01853.

Steele, M., & Boyd, T. (1998). Retreat of the cold halocline layer in the Arctic Ocean. *Journal of Geophysical Research*, *103*(C5), 10,419–10,435.

Steele, M., Ermold, W., & Zhang, J. (2008). Arctic Ocean surface warming trends over the past 100 years. *Geophysical Research Letters*, *35*, L02614. https://doi.org/10.1029/2007GL031651

Steele, M., Morison, J. H., & Curtin, T. B. (1995). Halocline water formation in the Barents Sea. *Journal of Geophysical Research*, *100*(C1), 881–894.

Stroeve, J., Holland, M. M., Meier, W., Scambos, T., & Serreze, M. (2007). Arctic sea ice decline: Faster than forecast. *Geophysical Research Letters*, *34*, L09501. https://doi.org/10.1029/2007GL029703

Stroeve, J. C., Serreze, M. C., Holland, M. M., Kay, J. E., Malanik, J., & Barrett, A. P. (2012). The Arctic's rapidly shrinking sea ice cover: A research synthesis. *Climatic Change*, *110*(3), 1005–1027. https://doi.org/10.1007/s10584-011-0101-1

Svellec, F., & Fedorov, A. V. (2016). AMOC sensitivity to surface buoyancy fluxes: Stronger ocean meridional heat transport with a weaker volume transport? *Climate Dynamics*, *47*(5), 1497–1513. https://doi.org/10.1007/s00382-015-2915-4

Svellec, F., Fedorov, A. V., & Liu, W. (2017). Arctic sea-ice decline weakens the Atlantic meridional overturning circulation. *Nature Climate Change*, *7*, 604. https://doi.org/10.1038/nclimate3353

Tietsche, S., Notz, D., Jungclaus, J. H., & Marotzke, J. (2011). Recovery mechanisms of Arctic summer sea ice. *Geophysical Research Letters*, *38*, L02707. https://doi.org/10.1029/2010GL045698

Walczowski, W., & Piechura, J. (2006). New evidence of warming propagating toward the Arctic Ocean. *Geophysical Research Letters*, *33*, L12601. https://doi.org/10.1029/2006GL025872

West, A. E., Keen, A. B., & Hewitt, H. T. (2013). Mechanisms causing reduced Arctic sea ice loss in a coupled climate model. *The Cryosphere*, *7*(2), 555–567.

Winton, M. (2003). On the climatic impact of ocean circulation. *Journal of Climate*, *16*(17), 2875–2889.

Winton, M., Griffies, S. M., Samuels, B. L., Sarmiento, J. L., & Frölicher, T. L. (2013). Connecting changing ocean circulation with changing climate. *Journal of Climate*, *26*(7), 2268–2278.

Xie, P., & Vallis, G. K. (2012). The passive and active nature of ocean heat uptake in idealized climate change experiments. *Climate Dynamics*, *38*(3–4), 667–684. https://doi.org/10.1007/s00382-011-1063-8

Yeager, S. G., Karspeck, A. R., & Danabasoglu, G. (2015). Predicted slowdown in the rate of Atlantic sea ice loss. *Geophysical Research Letters*, *42*, 10,704–10,713. https://doi.org/10.1002/2015GL065364